Politecnico di Torino

Politecnico di Torino

Master's degree in Biomedical Engineering

A.a. 2024/2025

Graduation Session July 2025

Design and 3D Printing of GelMA-Based Conductive Hydrogels for Wearable Strain Sensors

Supervisor:
Stefano Stassi

Candidate:
Carla Strada

Abstract

In this thesis, a conductive hydrogel based on Gelatin Methacryloyl (GelMA) was developed and thoroughly characterised for its application in flexible strain sensors and advanced 3D printing using Digital Light Processing (DLP) technology. Mechanical testing under tensile and compressive loads was performed, along with additional assessments of bending resistance, durability, and general degradability, in order to evaluate the material's structural integrity and long-term performance. The incorporation of tannic acid (TA) into the GelMA matrix significantly enhanced the mechanical properties, adhesion to various substrates, and printability of the hydrogel. Notably, the tensile strength of the hydrogel approximately doubled following TA addition, indicating a substantial improvement in robustness and resistance to failure under load.

Furthermore, TA facilitated improved interfacial bonding and shape fidelity during the printing process, allowing the fabrication of complex 3D geometries with high spatial resolution and structural stability. Optimisation of key DLP parameters—such as exposure time, layer thickness, and photoinitiator concentration—enabled reproducible printing of intricate constructs with fine detail and minimal distortion. These findings demonstrate that GelMA/TA composites represent a versatile and promising platform for the fabrication of next-generation wearable biosensors, combining biocompatibility, mechanical resilience, and compatibility with high-resolution additive manufacturing techniques.

Acknowledgements

Arrivare a scrivere questa pagina significa voltarsi indietro e riconoscere che ogni passo, ogni ostacolo superato, ogni gioia condivisa e ogni difficoltà affrontata non sono mai stati percorsi da sola. È un traguardo che porta con sé la somma delle persone che, in modi diversi, piccoli o immensi, mi hanno accompagnata, sostenuta, capita, spronata. A tutti loro va il mio grazie più sincero.

Inizio col ringraziare il mio relatore, il *Prof. Stefano Stassi*, per avermi guidata con disponibilità, attenzione e grande professionalità in questo percorso di tesi. La sua competenza e il suo entusiasmo sono stati fondamentali per la realizzazione di questo lavoro e per la mia crescita personale e accademica.

Un pensiero speciale va alla mia *mamma*, il mio esempio di vita e la mia roccia incrollabile. Ogni parola di incoraggiamento, ogni gesto di cura, ogni abbraccio nei momenti difficili sono stati per me linfa vitale. Non esistono abbastanza parole per esprimere quanto il suo amore, la sua forza, la sua dedizione e la sua presenza costante siano stati essenziali per arrivare fin qui. Senza di lei, nulla di tutto questo sarebbe stato possibile.

Alla mia *sorella*, compagna di vita insostituibile, che anche nel silenzio sa starmi vicina, che con uno sguardo sa comprendere senza bisogno di spiegazioni. La sua presenza è per me casa, certezza e rifugio. Ma è anche esempio di forza e determinazione: il suo carattere forte, deciso e autentico mi ha insegnato a non tirarmi mai indietro, ad affrontare le difficoltà con coraggio e ad andare avanti sempre, anche quando tutto sembra complicato. È grazie anche a lei se oggi mi sento più forte.

A mio *padre* e agli altri membri della mia famiglia, che hanno creduto in me anche quando io facevo fatica a farlo, che mi hanno insegnato il valore della perseveranza e che, con il loro affetto, hanno sempre reso il mio cammino più leggero.

Un ringraziamento profondo va a *Fabio*, per esserci sempre stato, con la sua

pazienza, il suo ascolto e la sua capacità di comprendere anche ciò che non veniva detto. La sua presenza costante, il suo sostegno silenzioso ma solido, e la sua capacità di starmi vicino nei modi più autentici mi hanno dato forza, conforto e fiducia. È stato un punto fermo, una presenza fondamentale che, soprattutto negli ultimi mesi, ha reso questo percorso più leggero, sereno e sorprendentemente felice.

A tutti i miei amici e a chi ha fatto parte di questo mio percorso, grazie. Per le risate, le parole giuste, le pause necessarie, le notti lunghe, le chiacchierate leggere e quelle intense. In particolare, voglio ringraziare:

Leonardo, che nonostante la distanza è sempre riuscito ad essere una delle persone più vicine a me. La nostra amicizia è un legame profondo, raro, che resiste al tempo e ai chilometri. La sua presenza, anche solo con un messaggio, è stata spesso più di quanto potessi chiedere.

Le mie migliori amiche di infanzia, *Claudia* (e un pensiero già colmo d'amore va alla piccola *Vittoria*, che sta per nascere e che già occupa un posto speciale nel mio cuore), *Leandra* e *Giorgia*. Con loro condivido un pezzo di vita che nessuno potrà mai toglierci, fatto di ricordi, crescita e un affetto che continua ad accompagnarmi ovunque vada.

Gli amici di una vita: *Pepi*, *Alex* e *Peppe*, persone su cui so di poter contare sempre. Il tempo e la vita possono cambiare tante cose, ma non la certezza che loro ci saranno, come lo sono sempre stati.

Gli amici del Messico: *Alafid*, *Giovanna*, *Eleonora* e *Alessia*, con cui ho condiviso l'esperienza più intensa, piena e bella della mia vita. Un capitolo di esistenza che mi ha trasformata. Un grazie speciale va a *Giovanna*, la mia *hermanita*, con la quale il legame è nato subito, spontaneo, profondo. Con lei ho trovato un'amicizia autentica, fatta di risate, confidenze e complicità che va oltre ogni confine.

Un grazie immenso alle mie coinquiline storiche: *Francesca*, *Elisa* e *Lucia*. Con loro ho condiviso case, cene improvvisate, notti di studio, risate incontenibili e una quotidianità fatta di piccoli gesti.

Un grazie di cuore anche ai luoghi di lavoro che sono diventati famiglia: il *Bevolution*, dove ho trovato non solo colleghi, ma amici sinceri, compagni di vita, persone che porterò sempre nel cuore; e il *Mated*, che ha segnato un altro capitolo importante del mio cammino.

Un pensiero lo dedico a *Torino*, che è diventata la mia seconda casa, il luogo che mi ha accolta, formato e fatto crescere. Ma anche alla mia *Sicilia*, che resterà sempre

la mia prima casa, il punto di partenza, la radice più profonda e insostituibile.

Infine, un ringraziamento che forse è il più difficile da scrivere, ma anche il più doveroso: a me stessa. A quella parte di me che non ha mai mollato, anche quando sarebbe stato più semplice farlo. A quella voce interiore che mi ha spinta a rialzarmi, a crederci ancora, a rimanere fedele ai miei sogni. Grazie per non esserti arresa.

Table of Contents

List of Figures

Chapter 1

Introduction

Wearable biomedical sensors represent a transformative advancement in healthcare technology, enabling continuous and non-invasive monitoring of physiological parameters. Among the key components of these devices are flexible strain sensors (FSS), which are capable of detecting mechanical deformations such as stretching and bending, offering high sensitivity, adaptability, and biocompatibility. Hydrogels, particularly those based on Gelatin Methacryloyl (GelMA), have emerged as ideal materials for such sensors because of their tunable mechanical properties, high water content, and compatibility with biological tissues. The incorporation of tannic acid (TA), a polyphenol with strong adhesive and crosslinking capabilities, further enhances the mechanical robustness and tissue adherence of these hydrogels. Recent developments in 3D printing, especially via Digital Light Processing (DLP), have enabled the precise fabrication of complex hydrogel-based structures, overcoming the limitations of conventional molding techniques. This thesis explores the fabrication of GelMA/TA-based hydrogel sensors, focusing on their chemical and mechanical characterization, followed by optimization for high-resolution 3D printing using DLP technology.

1.1 Wearable Biomedical Sensors

Biomedical sensors are among the most revolutionary technologies in the world of modern medicine and biomedical engineering. They are devices designed to detect, analyse and transmit data on physiological, biochemical or biomechanical parameters of the human body. They are used in many situations: from early diagnosis and constant monitoring of health conditions to real-time support during medical interventions or surgery. In simple terms, a biomedical sensor is a system that transforms a biological or physical signal, such as temperature, pressure, ion concentration or movement, into an electrical signal that can be read by electronic

devices.[1] A typical architecture of a wearable biomedical system for monitoring physiological parameters is shown in the figure 1.1. Sensors collect biological or mechanical data from the body, which are processed by a local control system. Subsequently, a communication module transmits the information to an external device, where the final processing and monitoring takes place. This modular structure enables the development of wearable devices such as smartbands and smartwatches, capable of providing continuous, non-invasive, real-time monitoring of health status. This ability to translate and communicate data makes sensors key tools for creating intelligent medical devices and for uniting the human body with digital technologies.[2] In recent decades, the development of biomedical sensors has made great strides. From the first, usually large, simple and rigid versions, they have progressed to more complex, small and highly integrated systems. Technologies such as microelectronics, new materials and advanced manufacturing methods have made it possible to create increasingly sophisticated sensors capable of functioning continuously, without being invasive, even in non-hospital settings. In particular, the use of materials that are flexible, biocompatible and easy to work with has opened the door to portable, wearable or even implantable devices. Thanks to recent advances in microfabrication and nanotechnology, these devices have become even more sensitive, precise and stable. The use of nanomaterials and micro- and nano-scale structures has improved the ability to respond to stimulation, while the development of more body-compatible platforms has facilitated their integration with biological systems [3]. For instance, Chang et al. developed a non-invasive,

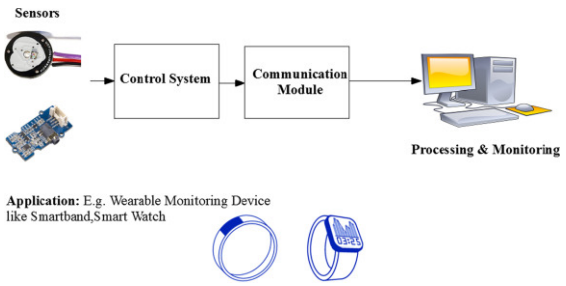

Figure 1.1: Biomedical system application example [1]

self-powered wearable biosensor for glucose monitoring in sweat, based on a flexible nanocomposite layer composed of nitrogen-doped graphene quantum dots (N-GQDs) and polyaniline (PANI) [Fig.1.2]. This innovative combination significantly enhanced surface charge density and electron transfer efficiency, resulting in improved triboelectric output and sensor sensitivity. The triboelectric sensor (TES) achieved a higher glucose detection sensitivity (23.52 mM-1) compared to its counterpart without N-GQD (16.44 mM - 1). Furthermore, the device operates without external power, highlighting its suitability for continuous real-time glucose

monitoring in portable healthcare applications [4].

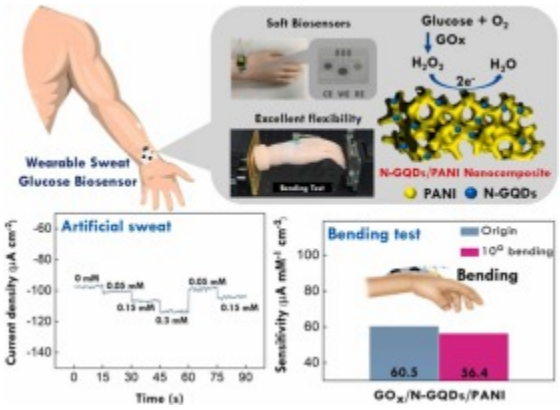

Figure 1.2: Bioensor architecture for glucose monitoring [4]

1.1.1 Flexible Sensors

Wearable electronics have revolutionised health monitoring, offering devices that can detect physiological parameters continuously and non-invasively. Flexible sensors are key components of these devices, as they can adapt to the surface of the human body, ensuring comfort and accuracy in data collection. In the context of wearable devices, flexible sensors offer significant advantages over traditional rigid devices. Thanks to their high sensitivity and ability to adhere perfectly to the skin, they can monitor vital signals such as blood pressure, heart rate and body temperature in real time. In addition, their elasticity allows them to detect body movements, speech and breathing, making them ideal tools for continuous health monitoring. [5] For the construction of flexible sensors, the materials used fall into three main categories: metals, carbon-based materials and polymers [6].

- Metals: this type of material are widely used due to their excellent electrical conductivity and the ability to be integrated into flexible structures. Common forms include metallic films such as gold and silver, metallic nanomaterials like nanowires and nanoparticles, liquid metals such as EGaIn, metal oxides like ZnO, and the more recently explored MXenes. Silver nanowires, for instance, are highly valued for their outstanding conductivity, transparency, and antibacterial properties, although they tend to entangle under mechanical stress [7]. Liquid metals like eutectic gallium-indium (EGaIn) combine biocompatibility and printability, making them particularly suitable for wearable devices [8]. Metal oxides, such as zinc oxide, offer good mechanical stability and sensitivity, making them promising for integration into smart textiles [9].

MXenes, thanks to their electrical conductivity and flexibility, have recently emerged as promising materials for piezoresistive sensors [10].

- Carbon-based materials: selected for their light weight, high flexibility, and excellent conductive properties. These include carbon black, carbon nanotubes (CNTs), and graphene (including graphene oxide). Carbon black is a cost-effective material that, when embedded in elastic polymer matrices, enhances electrical and mechanical properties, enabling the fabrication of sensors with high sensitivity and repeatability [11, 12]. CNTs, especially single-walled variants, offer superior conductivity, transparency, and structural uniformity, and are used to fabricate highly sensitive and stable resistive sensors [13]. Graphene and graphene oxide, due to their high surface area and two-dimensional structure, allow the construction of three-dimensional conductive networks, producing highly sensitive sensors adaptable to body surfaces [14].

- Polymers: this ones are primarily used as flexible substrates thanks to their thermal and chemical resistance, mechanical flexibility, and compatibility with conductive fillers. Polymers such as PDMS, PI, PU, PET, PVDF, and hydrogels are commonly employed as matrices for active sensing materials. The integration of conductive components into elastic polymer matrices enables the creation of high-performance resistive sensors. A noteworthy example is the use of Kapton as a substrate for boron-doped diamond nanosheets (BDDNS), which have been applied in sensors designed to detect low levels of strain [15].

Flexible Strain Sensors

In this context, flexible strain sensors (FSS) represent a promising technology for smart wearable devices due to their ability to detect large mechanical deformations such as bending, torsion and stretching and transform them into measurable signals. Compared to traditional metallic or semiconductor based devices, which detect limited deformations (<5%) and are inherently rigid, making them uncomfortable to wear, FSS offer advantages such as flexibility, light weight, biocompatibility, stability and high sensitivity, and are typically developed using conductive composites of elastomers, conductive liquids and stretchable optical fibres. These characteristics make them ideal for applications such as health monitoring, human movement detection, soft robotics and human-machine interfaces. Strain sensors find applications in various fields, including breathing and joint detection devices, robotic prostheses and muscle performance monitoring (figure 1.3) [16].

Yang et al. developed a highly sensitive and flexible pressure sensor designed for real-time monitoring of human motion. The sensor is based on a melamine fibre

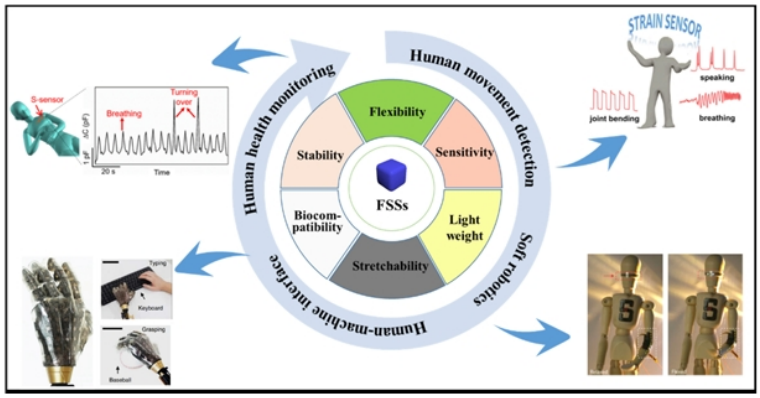

Figure 1.3: Summary of the properties and applications of flexible strain sensors [16]

substrate coated with MXene and PANI, materials that enhance its conductivity and surface properties, resulting in improved sensitivity and electrical contact. To further increase the contact area, a printed interdigital electrode was incorporated, enhancing the sensor's precision. The device exhibits a rapid response time of just 55 ms and a recovery time of approximately 50 ms. It can detect extremely low pressures, as little as 10.2 Pa, and maintains excellent performance over more than 10,000 usage cycles. Its flexibility and sensitivity make it particularly well-suited for integration into wearable devices or as artificial electronic skin [17] .

1.2 Hydrogels

Hydrogels are three-dimensional networks composed of hydrophilic polymers, capable of retaining significant amounts of water up to several hundred times their dry weight [18]. These structures are formed through physical or chemical crosslinking of natural or synthetic polymers, which gives them the ability to swell in aqueous environments; this is why they are often referred to as "hydrophilic gels". When fully dehydrated, hydrogels become 'xerogels', while controlled dehydration - such as by lyophilization - can lead to the formation of 'aerogels' with porosities up to 98% [19].

Hydrogels are generally classified into three classes: natural, synthetic, and semisynthetic.

- Natural hydrogels, such as those based on alginate, chitosan, collagen, or gelatin, are derived from biopolymers and exhibit excellent biocompatibility and intrinsic bioactivity, making them particularly attractive for biomedical applications such as wound healing and tissue engineering. However, their mechanical properties are often suboptimal, as they tend to be brittle and may degrade unpredictably under physiological conditions [20]. Their network architecture is generally less controllable, and their physicochemical stability may vary due to batch-to-batch variability of biological sources [21].

- Synthetic hydrogels, on the other hand, are engineered from monomers such as poly(ethylene glycol) (PEG), poly(vinyl alcohol) (PVA) or poly(acrylamide) and are distinguished by their wide range of sources of raw materials, high water absorption capacity, long-term stability, and greater structural tunability. These properties stem from the precise control of the chemical structure during synthesis [22]. From a mechanical standpoint, synthetic hydrogels demonstrate superior toughness and elasticity. For example, combining weak and strong crosslinks enables these materials to stretch up to 20 times their original length, while natural hydrogels may rupture only 1.2 times their initial length. This performance is attributed to covalent crosslinks that

prevent crack propagation and energy dissipation through reversible ionic crosslink rupture [23]. Additionally, their degradation behavior can be tailored by modifying the chemical structure, making them more susceptible to enzymatic or biological processes [24].

- Semi-synthetic hydrogels combine the advantages of both natural and synthetic systems by chemically modifying natural polymers or by incorporating synthetic moieties within a biopolymer backbone . This class of hydrogels allows for the preservation of biocompatibility and biological signalling, while simultaneously enabling tunability of mechanical stiffness and degradation profiles . Such tunable mechanical properties have been shown to influence critical cellular responses, such as neuronal growth and morphogenesis, indicating their potential for advanced regenerative medicine applications [25].

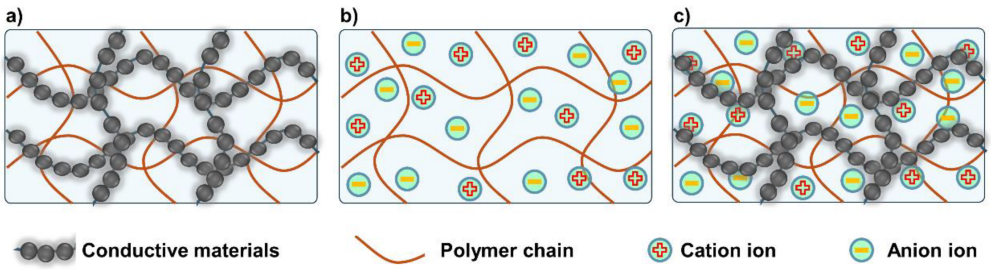

Figure 1.4: Conductive hydrogels: (a) electronic conductive hydrogels (ECH), (b) ion conductive hydrogels (ICH), and (c) composite conductive hydrogels (CCH) [26]

1.2.1 Conductive Hydrogels

In the context of soft electronics, biosensors and wearable devices, conductive hydrogels, i.e. functional materials characterized by adjustable elasticity and conductivity, are particularly studied [27, 28]. Depending on the mechanism by which they facilitate electrical transport, conductive hydrogels are commonly divided into three main types: electronic conductive hydrogels (ECH), ionic conductive hydrogels (ICH) and composite conductive hydrogels (CCH) [26] [Fig.1.4].

Electronic Conductive Hydrogels

ECHs are typically composed of a polymeric hydrogel matrix embedded with conductive agents, such as carbon-based nanomaterials (e.g., carbon nanotubes,

graphene), metal nanoparticles, or intrinsically conductive polymers such as PANI or PEDOT:PSS. These conductive networks, formed through chemical or physical crosslinking, enable efficient electron transport across the hydrogel. For instance, a graphene-based hydrogel produced via hydrothermal self-assembly exhibited a conductivity of $5 * 10^{-}3$ S/cm and a specific capacitance of 175 F/g [29] Similarly, PEDOT:PSS hydrogels fabricated by dry annealing followed by rehydration achieved conductivities up to 40 S/cm [30]. Despite their high conductivity, ECHs often display limited stretchability and poor toughness. Pure PEDOT:PSS hydrogels, for example, typically show only 35% elongation and negligible resistance variation under mechanical strain [30].

Liu et al. introduced an innovative "doping-then-gelation" strategy to fabricate a supramolecular poly(acrylic acid)/polyaniline (PAA/PANI) hydrogel featuring an entangled network structure [Fig.1.5]. The strong electrostatic interactions between the PAA and PANI chains act as dynamic crosslinks, promoting chain entanglement and enabling the hydrogel to exhibit exceptional stretchability (up to 2830%) and a high tensile strength of 120 kPa. Moreover, a PAA/PANI hydrogel-based sensor was developed, demonstrating high strain sensitivity (gauge factor, GF = 12.63), a fast response time of 222 ms, and reliable conductivity-based sensing performance under cyclic tensile loading[31].

Incorporating conductive fillers into robust hydrogel networks can improve mechanical properties, but at the cost of reduced conductivity due to filler aggregation or weak interfacial bonding [32, 33]. To this end, recent studies have introduced strategies such as in situ polymerization of conductive precursors within the hydrogel matrix to achieve a better balance between mechanical and electrical properties. Hydrogels formed with PAA and PANI, for example, have demonstrated tensile strains exceeding 2800%, along with high gauge factors and rapid response times [32]. Nevertheless, the conductivity in many such systems remains below 1 S/m [33].

Ionic Conductive Hydrogels

ICHs achieve conductivity via mobile ions rather than delocalised electrons. These hydrogels are synthesized by incorporating ionic species such as Na^{+}, K^{+}, or Cl^{-}into hydrophilic polymer matrices such as PAM, PAA, or PVA, which form ionic pathways or polyelectrolyte networks. Their soft consistency and low impedance at biological interfaces make them suitable for biocompatible and implantable devices [34].

Inorganic salts not only contribute to the electrical conductivity of hydrogel matrices but also play a significant role in tuning the mechanical properties of the polymer network. Two primary strategies are employed for introducing such salts into hydrogel systems.

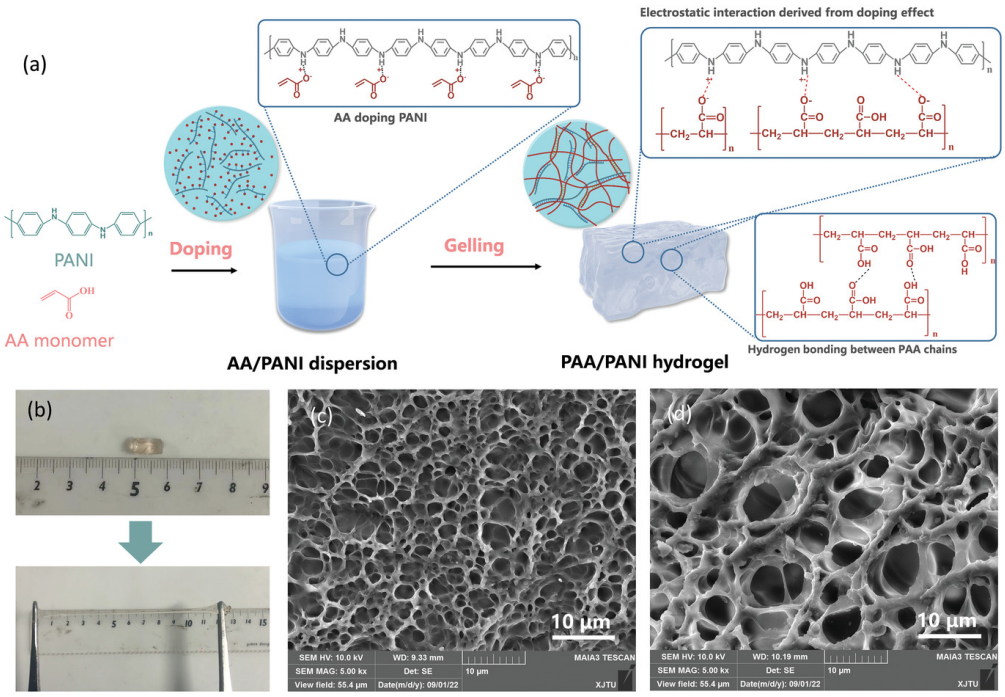

Figure 1.5: (a) Schematic illustration of synthesis process for PAA/PANI hydrogel; (b) The demonstration of excellent stretchability; SEM image of (c) PAA/PANI-3 hydrogel and d) PAA hydrogel [31]

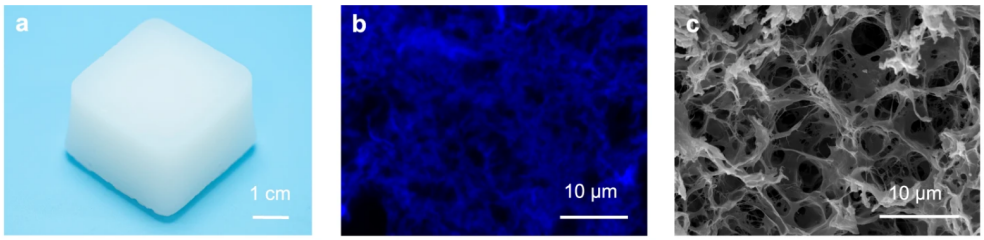

Figure 1.6: (a) Photograph of the Ion-CB hydrogel. (b) CLSM image of the Ion-CB hydrogel. (c) SEM image of the Ion-CB hydrogel shows the porous network. [35]

The first approach involves incorporating inorganic salts directly into the hydrogel precursor solution prior to polymerisation or crosslinking. This results in the formation of a gelled network with inherent conductive properties. For instance, Ding et al. developed an ionically conductive and mechanically robust hydrogel by forming a semi-interpenetrating polymer network composed of polyacrylamide (PAM), carboxymethyl chitosan, and sodium chloride (NaCl) . The addition of NaCl endowed the hydrogel with excellent ionic conductivity ranging from 0.52 to 6.44 S/m. Moreover, NaCl played a crucial role in inducing conformational changes in the carboxymethyl cellulose (CMC) chains, facilitating their extension and enhancing hydrogen bonding with the PAM network. This synergistic interaction resulted in superior mechanical performance, including high tensile strength (430 kPa), excellent elongation at break (1100%), and a reduced elastic modulus [36].

The second method, known as post-treatment, involves immersing the pre-formed hydrogel in a solution of inorganic salts or ionic liquids, allowing ions to diffuse into the crosslinked network. In a study by Chen et al., supramolecular hydrogels were fabricated through coordination interactions between cellulose and bentonite (BT), creating a stable reticulated framework. These neutral cellulose-BT hydrogels were subsequently soaked in an aqueous solution of lithium chloride (LiCl), resulting in the development of ionically conductive gels [Fig.1.6]. The final products exhibited outstanding mechanical properties, with a compressive strength of 3.2 MPa, and impressive ionic conductivity reaching 89.9 mS/cm [35]. However, the intrinsic high water content of ICHs poses challenges including dehydration, mechanical fragility, and weak tissue adhesion [28].

Composite Conductive Hydrogels

CCHs combine both ionic and electronic conductive elements, offering a pathway to synergistically enhance both conductivity and mechanical characteristics. A notable example of a composite conductive hydrogel (CCH) is a hybrid system based on graphene oxide (GO), trivalent metal ions (Fe^{3+}), and ionic salts, which exhibits outstanding electrical and mechanical properties. In this material, the two-dimensional structure of GO, rich in oxygen-containing functional groups, facilitates coordination interactions with Fe^{3+} ions, forming a three-dimensional crosslinked network that acts as the conductive matrix [Fig.1.7]. The incorporation of ionic salts (such as NaCl) further enhances the system's ionic conductivity by promoting charge transport through the hydrogel framework. This design enables a high electrical conductivity of up to 13.8 S/m, along with remarkable tensile strength and high strain sensitivity, key attributes for advanced applications in flexible sensors and wearable electronics.

Similarly, Liu et al. developed a composite conductive hydrogel (CCH) by integrating a "soft" homogeneous polymer network composed of poly(vinyl alcohol)

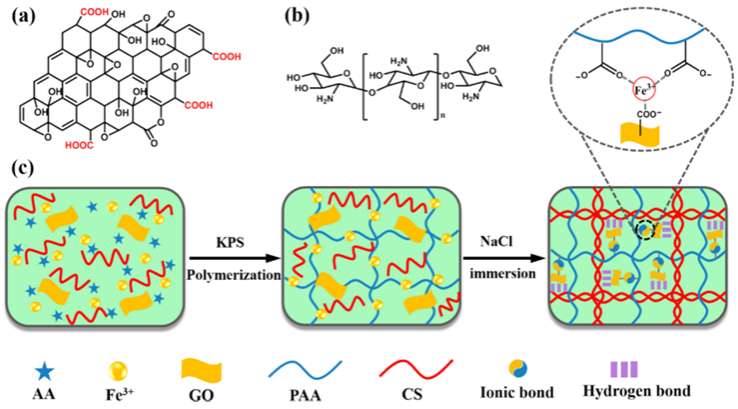

Figure 1.7: (a) Chemical structure of GO; (b) Chemical structure of CS; (c) Schematic showing the synthetic process and mechanism of $PAA/GO - Fe3^{+}$ hydrogel formation. [37]

(PVA) and poly(vinylpyrrolidone) (PVP) with a "hard" nanoreinforcing network based on cellulose nanocrystals (CNCs) dynamically crosslinked via Fe^{3+} ions. This synergistic architecture, inspired by biological soft tissues, allowse material to combine excellent mechanical strength (up to 2.1 MPa of tensile stress), outstanding stretchability (up to 830%) remarkable fracture toughness (up to 8.9 MJ/m^3), while also offering rapid self-healing capability int external stimuli. The dynamic CNCs–Fe^{3+} coordination bonds act as sacrificial links to dissipate energy under stress, whereas the homogeneous polymer phase ensures smooth stress transfer and elastic recovery. Moreover, the hydrogel exhibits highly sensitive and repeatable strain-responsive electrical behaviour, making it ideal for wearable strain sensors capable of detecting subtle physiological signals such as joint motion, respiration, and pulse variations.[38]

In general, ECHs provide higher electrical conductivity than ICHs, due to their reliance on electronic rather than ionic charge transport mechanisms. However, this enhanced conductivity often comes at the expense of mechanical flexibility and stretchability. CCHs aim to bridge this trade-off by integrating both electronic and ionic conductive phases, enabling a tunable balance between electrical performance, mechanical compliance, and sensitivity for specific sensing applications [26].

Based on the classification discussed above, the hydrogel sensor developed in this work is best categorised as an ionic conductive hydrogel (ICH). The electrical conductivity arises from the migration of sodium and chloride ions (Na^+/Cl^-) dissolved in the aqueous–glycerol phase, rather than from electron transport mechanisms.

Unlike electronic or composite conductive hydrogels, the present formulation does not contain intrinsically conductive polymers (e.g., PEDOT:PSS, PANI) or carbon-based fillers. Instead, its conductivity is enabled exclusively by the ionic mobility within the hydrogel matrix. The presence of glycerol serves to reduce water evaporation and increase durability, while the addition of tannic acid improves mechanical strength and printability without altering the underlying ionic conduction mechanism.

Therefore, although the material integrates functional additives such as glycerol and TA, its charge transport relies entirely on mobile ions, placing it firmly within the ICH category.

1.2.2 Tannic Acid

Tannins, a class of polyphenolic compounds commonly found across the plant kingdom, have attracted significant scientific interest due to their notable biological activities, including antioxidant, anti-mutagenic, anti-carcinogenic, and antibacterial effects. Tannic Acid (penta-m-digallolyl glucose) (TA) based on the commercial formula $C_{76}H_{52}O_{46}$ [Fig. 1.8], involves a large number of reactive functional groups, such as hydroxyl and phenolic hydroxyl. Among the various

applications explored, TA has emerged as a valuable component in the development of bioadhesive hydrogels. This is largely attributed to its high content of polyphenol groups, which enable extensive crosslinking and facilitate strong adhesion to a wide range of biological and synthetic substrates.[39]. To exploit the strong adhesive

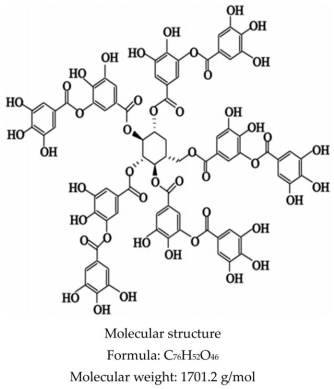

Figure 1.8: Molecular structure of TA [40]

potential of TA, numerous studies have investigated the design of tannin-based hydrogels. Lee et al. developed an innovative medical adhesive called TAPE (Tannic Acid-Polyethylene Glycol Adhesive), obtained by hydrogen bonds between tannic acid (TA) and polyethylene glycol (PEG). This adhesive hydrogel, easily realised without additional chemical reactions, showed 250% higher adhesive strength than fibrin glue, maintaining good performance even in an aqueous environment. In addition, TAPE demonstrated haemostatic properties and biocompatibility, making it suitable for applications in surgery and tissue healing. [41] Various studies have shown that the addition of TA not only improves the adhesion of the hydrogel but also significantly increases the mechanical properties of the hydrogel. With regard to improvement in mechanical performance, the study by Haofei Qie et al. showed that the addition of tannic acid (TA) to the gelatin-polypyrrole/polyacrylamide (G-PPy/PAAm-TA) hydrogel system had a crucial impact. The improvement in the mechanical properties of the hydrogel studied was confirmed by tensile measurements as shown in Fig. 1.9. The PAAm hydrogel alone has good ductility but low strength (95 kPa). The addition of the composite G-PPy increases the strength (130 kPa) but reduces the elongation. With the addition of tannic acid (TA), the strength increases dramatically to 1.44 MPa, while maintaining good deformability. Overall, the PAAm/G-PPy/TA system shows a mechanical increase of up to 15 times compared to pure PAAm. With a 10% addition of TA, the hydrogel achieved a maximum tensile strength of 1.44 ± 0.11 MPa, with an increase in elastic modulus from 74 ± 3 kPa to 138 ± 5 kPa and an increase in toughness to 2.58 ± 0.45 MJ/m^3. [42]. The study by Zhao et al. demonstrated that, due to

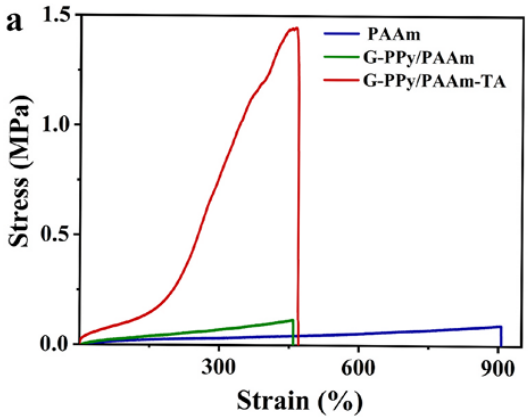

Figure 1.9: Tensile stress-strain curves of PAAm hydrogel, G-PPy/PAAm hydrogel, and G-PPy/PAAm-TA hydrogel [42]

the inclusion of catechol groups from tannic acid, the PAMT hydrogel achieved a maximum adhesion strength of 48.01 N/m on glass, compared to 69.20 N/m for the hydrogel without TA. This adhesive strength remained high on various surfaces, such as plastic and wood [Fig.1.10], making the material suitable for applications in wearable sensors and detection devices. Furthermore, the hydrogel can be removed from the skin without leaving any residue, confirming its excellent adhesion and compatibility with biological substrates [43].

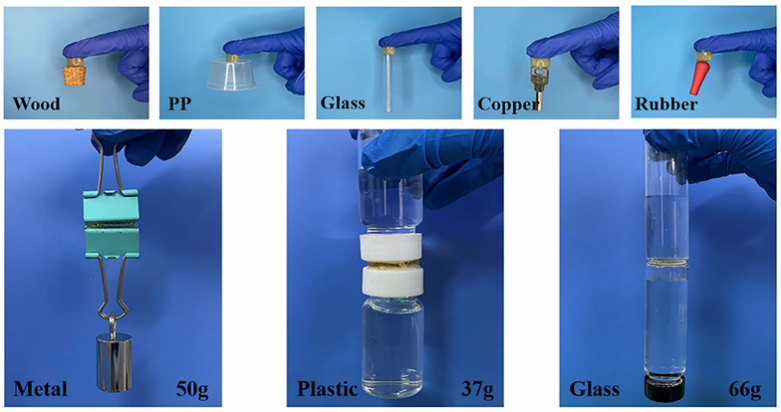

Figure 1.10: Digital photographs showing the adhesion of the hydrogel to various substrates [43]

1.3 GelMA sensors

Gelatin methacryloyl (GelMA) is a methacrylated biopolymer derived from gelatin, which in turn can be sourced from porcine or fish skin [44]. When hydrated, GelMA forms a crosslinked hydrogel network via photopolymerisation in the presence of water. This hydrogel exhibits excellent biocompatibility compared to many other synthetic hydrogel systems and has been extensively applied in various biomedical fields, particularly in tissue engineering (including bone, cartilage, cardiac, and vascular tissues). It is also widely used in fundamental research for studies on single cells, cell signalling, drug and gene delivery, and biological sensors. GelMA's success in these applications is due to its biocompatibility and ability to mimic the natural 3D environment of cells, facilitating cell growth and tissue regeneration. In fact, these hydrogels mimic some essential properties of the native extracellular matrix (ECM), such as the presence of metalloproteinase-responsive peptide motifs and cell-binding sites, promoting cell proliferation and spreading [45]. Fig. 1.11 illustrates the structure of GelMA, highlighting the site of modification within the gelatin molecule, which is associated with the naturally

occurring RGD (arginine-glycine-aspartic acid) sequence. The introduction of methacrylic anhydride results in the attachment of methacryloyl groups to the amino residues of gelatin. These functional groups allow covalent cross-linking by radical polymerization in the presence of a photoinitiator.[46] In addition, GelMA

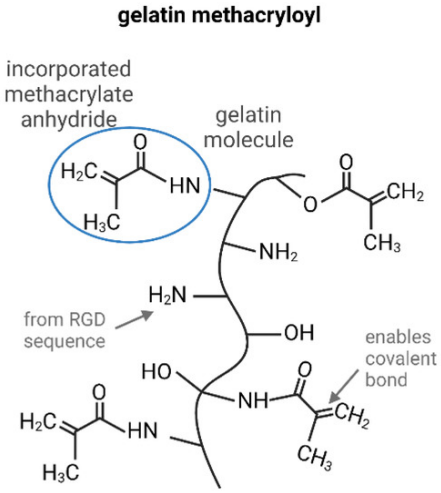

Figure 1.11: GelMA with modificated sides[47]

has a Young's modulus similar to human tissue, which can contribute to excellent biomechanical coupling in electronic-tissue interfaces. Its mechanical properties are also highly tunable, allowing GelMA-based devices to meet different mechanical stiffness requirements in practical applications. Importantly, GelMA has excellent toughness, allowing it to recover its original shape after compression. In addition, GelMA has good transparency, making it an ideal candidate for the development of fully transparent bioelectronics. These properties make GelMA a promising hydrogel for the development of highly sensitive, skin-friendly, biocompatible and transparent wearable sensors.[48]

Zhang et al. developed a wireless, passive magnetic strain sensor based on a magnetic hydrogel composed of GelMA and magnetic Fe3O4 nanoparticles [Fig. 1.12]. This sensor aims to monitor subtle biomechanical forces in real time, demonstrating potential for applications in biocompatible implants for mechanical tissue monitoring. GelMA was chosen for its excellent biocompatibility and its ability to form hydrogels with soft tissue-like mechanical properties through a UV light-induced cross-linking process. The addition of Fe_3O_4 nanoparticles improved the magnetic properties of the gel, making it suitable for wireless biomechanical monitoring. GelMA, at a concentration of 5%, maintained a Young's modulus of 1.2 kPa, which is comparable to that of biological tissue, and showed long-term stability in saline solutions for more than 20 days, with a detection sensitivity

of up to 50 µm strain. The magnetic properties of the sensor increased with the Fe_3O_4 concentration, reaching a maximum magnetization of 12.74 emu/g for a concentration of 15 mg/ml [49].

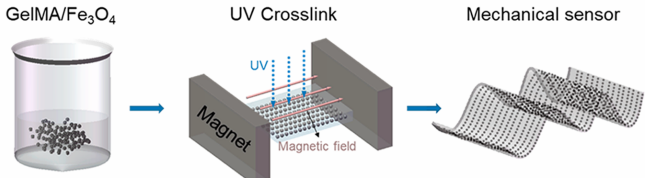

Figure 1.12: Schematic illustration of a magnetic-based strain sensor [49]

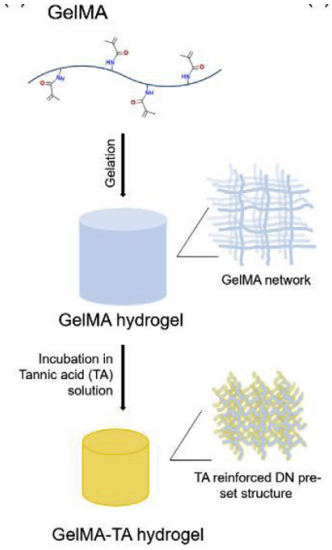

Figure 1.13: The schematic illustration of preparing multifunctional GelMA-TA hydrogel [50]

Liu et al. developed a double-network (DN) hydrogel based on GelMA and reinforced with tannic acid (TA) [Fig. 1.13], exhibiting excellent elasticity, self-healing capabilities, and underwater adhesion. These features enable its use in the fabrication of a self-regenerating electronic skin with strain-sensitive conductivity, further enhanced by the incorporation of multi-walled carbon nanotubes (MWCNTs). The introduction of TA into the GelMA matrix significantly improves the mechanical performance, increasing both the compressive modulus and tensile properties, thus making the hydrogel more flexible and robust. TA also enhances the adhesive properties of the material, albeit at the expense of a reduction in overall volume. Cytocompatibility tests demonstrated a high degree of biocompatibility, while in vivo experiments confirmed that the GelMA-TA hydrogel performed effectively

in closing surgical incisions on both skin and gastric tissue without the need for sutures[50].

1.4 3D printing of sensors

To evaluate the practicality of electrically conductive hydrogels in flexible electronics, traditional fusion and templating techniques are commonly employed to generate suitable structures .However, reliance on moulds, dies, or masks in these processes restricts customisation, resulting in the production of only basic 3D structures [51]. Additionally, the gelation method requires a substantial volume of liquid precursors for in situ solidification, leading to significant energy and resource consumption. Moreover, it has been demonstrated that the performance of flexible electronics can be enhanced through meticulous structural design, such as the incorporation of hierarchical internal architectures at the micro- and nanoscale [52]. To address these challenges, 3D printing is considered the most effective method for engineering complex and precise 3D structures. The use of 3D printing enables the precise fabrication of stretchable hydrogels with intricate 3D designs, structural combinations, and superior functionalities [53].

The term "3D printing" encompasses a suite of advanced technologies that enable the layer-by-layer construction of three-dimensional components from computer-generated models [54]. The origins of this technology can be traced back to the 1980s, with the development of stereolithography (SLA), a technique that utilises an ultraviolet (UV) laser to cure successive layers of liquid photopolymer resin. Subsequently, towards the late 1990s, other 3D printing techniques such as fused deposition modelling (FDM) and selective laser sintering (SLS) emerged, facilitating the fabrication of 3D objects through sequential layering from digital files [55]. The incorporation of hydrogels into the 3D printing process, which gained momentum in the early 2010s, has further expanded the capabilities of this technology by enabling the creation of complex hydrogel-based structures. These developments have revolutionised various sectors, particularly in the biomedical field, by allowing the fabrication of biomimetic architectures suitable for applications such as tissue engineering and controlled drug delivery [56]. Compared to conventional manufacturing techniques, 3D printing offers several inherent advantages, including substantial design flexibility, rapid prototyping capabilities, reduced material waste, the ability to produce customised objects on demand, and often enhanced cost-effectiveness. However, there are still some obstacles, including material properties (viscosity, thixotropy), crosslinking methods, multi-material printing, cost-effectiveness, printing resolution, and structural integrity, that must be addressed to advance 3D printing capabilities with gels [26]. The 3D printing process begins with creating a three-dimensional model using CAD software or by employing reverse engineering

through a 3D scanner . The model is then sliced into cross-sectional layers, which are transferred to the printer. The printer subsequently constructs the object by sequentially depositing material layers, much like an inkjet printer building up material step by step. As shown in the Fig. 1.13, this process generally involves three main phases: modeling, printing and finishing.

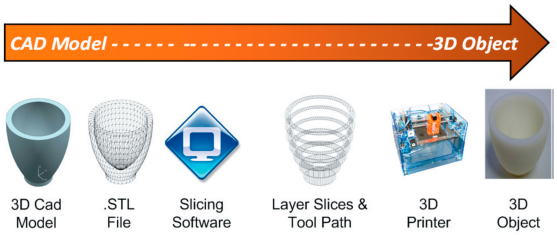

Figure 1.14: The 3D printing process [57]

For the creation of conductive hydrogels, a number of 3D printing techniques have been developed; each has unique benefits and drawbacks based on the intended use. Inkjet printing, digital light processing (DLP), two-photon polymerization (TPP), direct ink writing (DIW), and stereolithography (SLA) are the main techniques.

- Inkjet Printing: this technique employs low-viscosity fluid inks that are deposited onto a substrate as discrete droplets. Solidification is typically achieved through ultraviolet (UV) curing or thermal processes [58]. This technique is particularly suited to high-resolution deposition of conductive inks, enabling fine features with dimensions typically in the range of 20–50 µm [26]. It is ideal for producing thin, intricate layers of material with precise patterning. However, the low viscosity of the ink can limit the ability to create self-supporting structures, which may compromise the overall mechanical integrity and feature definition. Moreover, the formulation of the conductive ink is critical to achieving the desired conductivity and print fidelity [59].

- Direct Ink Writing (DIW): a versatile 3D printing technology that utilises viscous solutions or gels extruded through a nozzle to build three-dimensional structures. This method supports a wide range of materials with tunable rheological properties, facilitating the creation of custom conductive hydrogel formulations. Typically, feature resolutions for DIW structures lie in the range of 100–300 µm [26]. While DIW excels in material adaptability and customisation, it often necessitates the use of temporary support materials to prevent structural collapse during printing, adding complexity to the manufacturing process [60].

- Two-Photon Polymerisation (TPP): TPP leverages the simultaneous absorption of two photons to initiate polymerisation within photosensitive hydrogel precursors, enabling the creation of three-dimensional structures with sub-micron resolution. This approach is particularly advantageous for applications requiring nanoscale features, as it achieves resolutions below 1 µm [26]. Nonetheless, TPP is constrained by high equipment costs, the need for specialised photoinitiators compatible with the hydrogel matrix, and limited material choices, which can restrict its widespread adoption despite its exceptional precision.

- Stereolithography (SLA): SLA employs a focused UV laser to solidify successive layers of liquid photopolymer resin, producing objects with high resolution and excellent feature definition. This technique is renowned for its ability to generate complex structures with microscale detail, typically achieving resolutions in the range of 50–200 µm [26]. However, SLA printing is inherently slow, as it solidifies the resin voxel by voxel, resulting in longer production times compared to projection-based methods. Moreover, the resins used in SLA must possess excellent optical transparency and favourable rheological properties, which can limit material options. A notable application of SLA is in the fabrication of composite ionic conductive hydrogels, which exhibit superior mechanical strength and electrical conductivity by incorporating doped photopolymers [60].

- Digital Light Processing (DLP) is a 3D printing technique that, like stereolithography (SLA), uses light to photopolymerize resins, but differs fundamentally in implementation. Instead of point-by-point curing, DLP projects two-dimensional images of each layer using digital micromirror devices (DMDs) or liquid crystal displays (LCDs), resulting in significantly higher print speeds [61]. This approach allows for the efficient fabrication of complex, conductive hydrogel structures, which is particularly relevant for advanced biomedical sensor applications. Notably, DLP achieves high printing resolutions in the range of 25–100 µm while maintaining elevated production speeds. Furthermore, DLP-compatible photopolymer resins can be formulated by incorporating conductive powders or fibers, thereby facilitating the development of electrically active hydrogels [26]. However, DLP requires careful selection of photoinitiators and resin formulations, faces material compatibility constraints, and often needs post-processing to remove residual resin and ensure complete polymerization [26]. In this thesis, I am focusing on DLP-based fabrication due to its high resolution, support for complex geometries, and its potential to integrate conductive fillers into hydrogel systems—making it ideal for developing advanced strain sensors.

1.4.1 3D Printing of Hydrogel

For flexible sensors, 3D printing with Digital Light Processing (DLP) technology has established itself as an effective technique for the production of complex, high-resolution structures, essential for sensor integration. In particular, as already mentioned, hydrogels, with their high water content and tunable mechanical properties, are key materials for flexible sensors, offering biocompatibility and responsiveness to stimuli, making them ideal for biomedical interfaces. For this reason, in recent years several studies have demonstrated that 3D printing of hydrogels based on DLP technology enables the creation of flexible and wearable sensors with increased sensitivity and mechanical durability [52].

The study by Guo et al. uses 3D printing by Digital Light Processing (DLP) to fabricate conductive and degradable hydrogels for epidermal sensors. The UV polymerization of N-acryloylmorpholine (ACMO) allows to obtain complex structures with high precision and rapid gelation (1.4 seconds). DLP printing provides high resolution, with precision down to 0.88 mm in the first layer as shown in the figure. Ion sputter coating of platinum particles provides a conductivity of 1.6 S/cm in just 2 minutes. The resulting hydrogel exhibits excellent elongation (up to 1781.5%) and mechanical strength, maintaining structural stability during repeated stress cycles. The sensor, with a gauge factor of 1.5 at low strains and 7.2 at high strains, can accurately monitor joint movements and subtle body vibrations, such as swallowing. Furthermore, the device completely degrades in 5 hours in gastric juice and 10 days in soil, representing an eco-friendly and sustainable solution for wearable electronics [51].

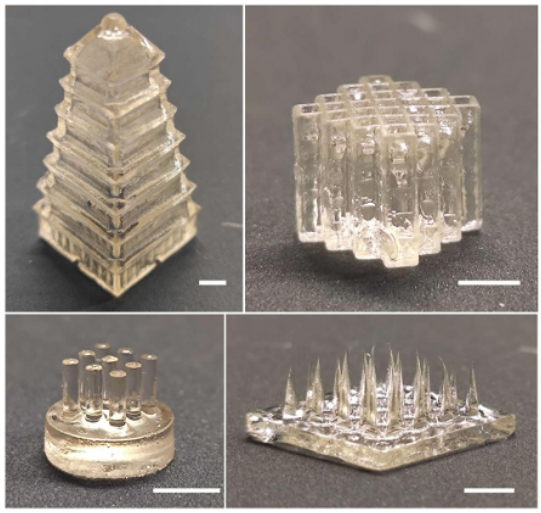

Figure 1.15: Photographs of poly(ACMO) components with complex config urations. Scale bars, 5 mm [51]

Caprioli et al. developed a self-healing hydrogel system using Digital Light Processing (DLP) 3D printing, enabling the fabrication of complex, self-repairing hydrogel structures. The hydrogel formulation comprises a semi-interpenetrating polymer network (semi-IPN) of poly(vinyl alcohol) (PVA) and a crosslinked acrylic matrix, using only commercially available materials. The DLP process employed a water-based ink containing PVA, acrylic acid (AAc), and PEGDA, allowing the creation of intricate 3D architectures with excellent shape fidelity and feature resolution. Notably, the hydrogel demonstrates rapid self-healing at room temperature, achieving 72% recovery of initial tensile strength after 12 hours, without external stimuli (Fig. 1.16). The study highlights the potential of DLP for fabricating advanced soft materials for applications in biomedicine, robotics, and flexible sensors [62].

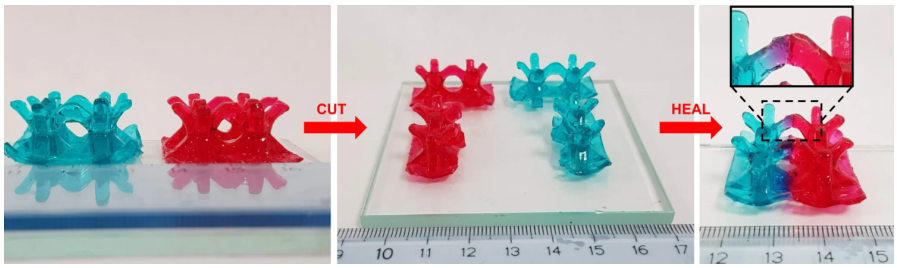

Figure 1.16: Body-centred cubic lattice structures were printed with red and green dyes, showing clear dye diffusion at the interface after 12 hours.[62]

GelMA printing

Within the hydrogel family, gelatin methacryloyl (GelMA) has gained considerable attention due to its ability to form stable crosslinked networks via photopolymerisation, while preserving the intrinsic biofunctionality of natural gelatin [63]. Owing to its biocompatibility, photocrosslinkability, and tunable physicochemical characteristics, GelMA has been widely employed in various tissue engineering applications, particularly in the context of 3D bioprinting. Its capacity to undergo rapid photocuring under controlled conditions enables the fabrication of hydrogel scaffolds with spatially defined architectures and adjustable mechanical properties, offering a favourable environment for cellular adhesion, proliferation, and differentiation.

Indeed, GelMA hydrogels have been extensively used in the regeneration of diverse tissues—such as cartilage, bone, muscle, skin, and myocardium—and in the development of in vitro models for drug screening, disease modelling, and personalised medicine. Additionally, GelMA has found application in drug delivery

systems and in biofabrication strategies for constructing complex multicellular structures and organ models [63, 64].

Despite its widespread use in biomedical research, GelMA remains relatively underexplored in the field of wearable and flexible sensors. Nevertheless, its biocompatibility, photocrosslinkability, and tunable network properties make it a compelling candidate for the development of soft and adaptive sensing platforms. This thesis investigates the potential of GelMA-based hydrogels for applications beyond conventional tissue engineering, with a particular emphasis on their formulation and printability. The objective is to assess their suitability for advanced fabrication strategies such as additive manufacturing, aiming to develop materials that combine structural integrity with the flexibility required for emerging applications in bioengineering and soft materials.

Parameters that influence the printability of GelMA, especially in 3D bioprinting, include:

- Hydrogel viscosity: The viscosity of GelMA is a key rheological parameter to achieve effective extrusion during printing. Optimization of viscosity can be achieved by varying the GelMA concentration, temperature, and degree of cross-linking [45]. In general, the optimal viscosity for bioprinting is between 100 and 1000 Pa/s [52].

- Polymer concentration: The concentration of GelMA directly influences the viscosity and the ability to form stable structures. Typical concentrations for bioprinting range from 5% to 15% by weight, with concentrations below 5% possibly not forming a sufficiently stable gel [64]. A study by Sharifi et al. (2021) demonstrated that increasing the concentration of GelMA from 10% to 25% significantly improved the mechanical properties of hydrogels, with an increase in tensile and compressive strength. However, higher concentrations of GelMA reduced swelling and increased resistance to enzymatic degradation. From a biocompatibility perspective, lower concentrations (10–15%) promoted cell growth, while higher concentrations (20–25%) limited cell spreading and proliferation due to excessive stiffness. Therefore, the optimal concentration depends on the balance between mechanical robustness and cell growth promotion [65].

- Porosity and pore size: The porosity of GelMA can be adjusted to influence cell distribution and penetration into printed fabrics. The pore size can range from micropores (50–100 µm) to macropores (200–700 µm), depending on the concentration and additional components used in the bioink [63]. GelMA–micro/nano hydroxyapatite (HAp) composite hydrogel scaffold was 3D printed using digital light processing (DLP) to form a porous matrix for bone tissue regeneration. The porosity of the scaffold was adjusted by

changing the concentration of GelMA, the degree of GelMA substitution, and the addition of micro/nano–HAp. In vitro biocompatibility studies of the 3D printed scaffold showed good cell adhesion, osteoblastic cell proliferation, and osteogenic differentiation. In an in vivo animal model using rabbits, the 3D printed cellular scaffold showed new bone formation in critical bone defects in the skull [66].

- Photoinitiators and UV crosslinking: Photocrosslinking of GelMA requires photoinitiators that enable crosslinking under exposure to specific light wavelengths. The study by Khoon Lim et al. demonstrated that photoinitiator concentration and light intensity influence the mechanical properties of GelMA hydrogels and cell viability. Increasing the Ru/SPS concentration from 0.1/1 to 0.2/2 mM/mM improved the polymerization rate and mechanical strength, reaching a compressive modulus of 31.6 kPa. However, higher concentrations did not show additional benefits. In terms of cell viability, the Ru/SPS system under visible light preserved cells better, with a viability of more than 85% after 35 days, compared to the UV system, while also reducing phototoxicity and improving metabolic activity [67]. Similarly, Sharifi et al. (2021) investigated the use of Eosin Y (EY) as a photosensitizer for the crosslinking of GelMA hydrogels with visible light, compared to traditional UV systems, known for their phototoxicity. EY, combined with TEOA and VC, was optimized to obtain hydrogels with optimal mechanical properties. EY concentrations of 0.05 mM and exposure to white LED light (20 mW/cm^2) for 4 min provided the best results. However, high concentrations of photoinitiators showed cytotoxic effects, reducing cell viability. The study demonstrates that the use of visible light is an effective and safe alternative for biomedical applications, provided that the concentrations are carefully optimized [65].

The article by Pepelanova et al. demonstrates the versatility of GelMA as platforms for three-dimensional cell culture and extrusion bioprinting in tissue engineering. GelMA, obtained by the modification of gelatin with methacrylate groups, exhibit excellent biocompatible properties, essential to support the adhesion and proliferation of adipose-derived mesenchymal stem cells (hAD-MSC). The synthesis process and polymerization parameters, such as UV irradiation concentration and conditions, are controlled to optimize the mechanical properties of the gel. In particular, the use of gels at concentrations of 5% (w/v) and a crosslinking intensity of 1.2 J/cm^2 have been shown to promote good cell proliferation. Furthermore, the addition of biocompatible additives, such as alginates and silicate nanoparticles, improved the viscosity of the gels, favoring the printability and resolution in 3D bioprinting (Fig. 1.17). The results highlight that the modified GelMA gels

possess a shear thinning behavior, facilitating the deposition during printing and maintaining the fidelity of the final shape [68].

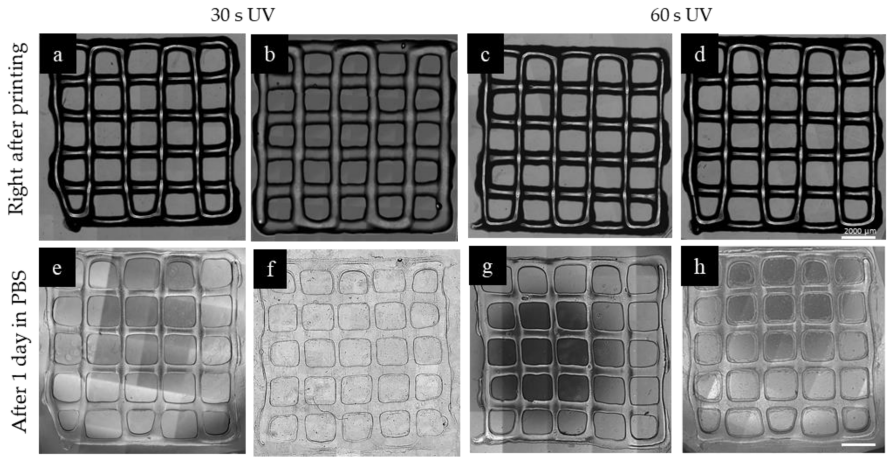

Figure 1.17: Two-layered 3D-printed constructs were fabricated with varying UV crosslinking times (30 or 60 s) and optional 30 min mTGase treatment. The addition of mTGase reduced swelling and improved shape fidelity.[68]

A recent study by Shi et al. explored the use of collagen methacrylate (CMA)-based bioinks as an alternative to gelatin methacrylate (GelMA) in 3D bioprinting applications. GelMA, although widely used, suffers from denaturation of the native collagen triple helix structure during processing, thus reducing its ability to support critical cell-matrix interactions. To overcome these limitations, the authors developed an improved CMA synthesis protocol, which preserves the triple-helix structure and consequently improves its bioactivity. In the study, CMA-based bioinks were prepared and evaluated for their printability and biological performance using both digital light-based printing (DLP) and extrusion bioprinting. For DLP printing, as shown in Fig. 1.18 CMA demonstrated superior shape fidelity compared to GelMA, with smoother surfaces and improved resolution. The study optimized the photoinitiator concentration (0.5% LAP) and the CMA content (2wt%) to achieve rapid gelation and robust scaffold formation, with a light intensity of approximately 1.69 mW/cm^2, similar to typical DLP conditions[69].

Cell-containing hydrogels were fabricated by incorporating Schwann cells (SCs) and bone mesenchymal stem cells (BMSCs) into CMA-based bioinks. The results revealed significantly higher cell viability (>90%), better spreading, and superior proliferation in CMA hydrogels compared to those in GelMA constructs. Furthermore, the expression of key genes related to neural regeneration and osteogenesis were upregulated in CMA-based systems, highlighting the potential of CMA in promoting tissue-specific functionality. Interestingly, although GelMA achieved

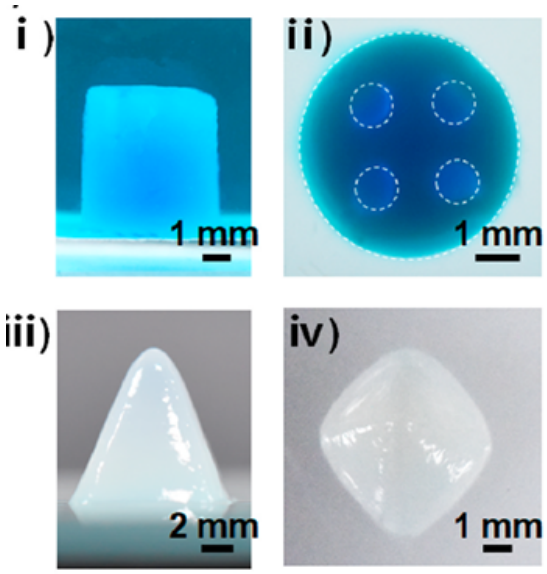

Figure 1.18: Various 3D-printed CMA-based hydrogel structures: (i)cylinder, (ii)multichannel disc, (iii) triangular pyramid and (iv)quadrangular pyramid, fabricated using DLP.[69]

high levels of methacrylation (98%) and good printability, it still failed to match the biological performance achieved with CMA, indicating that preserving the native collagen structure is critical for effective cellular interactions [69].

The study by Jia et al. uses Digital Light Processing (DLP) 3D printing to fabricate multicrosslinked hydrogel scaffolds based on GelMA, HAMA and PAM, intended for nasal cartilage regeneration. In this study, each layer was irradiated with 405 nm light for 10 seconds, with an intensity of 5 mW/cm^2, allowing for rapid and controlled polymerization. The precision achieved, with a line width of 300 µm and a spacing of 700 µm, ensures that the printed structures are faithful to the designed 3D models, offering scaffolds with complex geometries and high structural stability (Fig. 1.19). Furthermore, GelMA/HAMA/PAM scaffolds showed improved mechanical properties, with a compressive modulus of 0.182 MPa, and excellent biocompatibility, promoting cell proliferation and differentiation in chondrocytes [70].

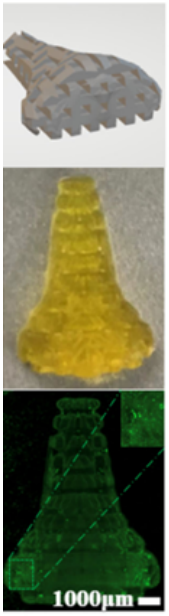

Figure 1.19: 3D-printed nasal hydrogel scaffold (model and optical image) and live-dead staining of cells at Day 7 show cell viability in the printed construct. [70]

The study by Li et al. uses an innovative approach of adjustable precuring in Digital Light Processing (DLP) 3D printing to improve the fidelity and efficiency of printing, especially for photopolymerizable hydrogels such as GelMA. The method involves two steps: an initial prepolymerization that allows a gel to remain in a pregelled state, followed by a complete polymerization. This approach significantly reduces the total printing time (only 5.6% compared to conventional DLP methods

with 10.1 μm layer thicknesses), improving the surface quality and minimizing the "staircase" effect typical of additive techniques. GelMA, used as a bioink for printing, has been shown to support increased cell viability when bioprinted with this method. PC12 cells incorporated in GelMA showed a viability of $90.2 \pm 6.1\%$ compared to $54.5 \pm 4.8\%$ obtained with traditional DLP methods, thanks to the reduction of UV exposure and the more precise control of polymerization [71].

Chapter 2

Materials and Methods

2.1 GelMA-based hydrogel synthesis

2.1.1 Synthesis of Gelatin Methacryloyl (GelMA)

GelMA was synthesised following a method previously reported by Vigata et al. [72], with modifications introduced to optimise the methacrylation reaction.

1. **Preparation of gelatin solution:** 40 g of cold-water fish gelatin (Sigma-Aldrich, Darmstadt, Germany), corresponding to 20% w/v, were dissolved in 200 mL of distilled water at neutral pH and room temperature (RT), using a magnetic stirrer (AREX-6, Velp Scientifica). Complete dissolution was achieved in approximately 40 minutes.

2. **pH adjustment:** Once a clear solution was obtained, the pH was adjusted to 9 using a 3 M NaOH solution, prepared by dissolving 12 g of sodium hydroxide in 100 mL of distilled water.

3. **Methacrylation:** Methacrylic anhydride (MA; Sigma-Aldrich) was added dropwise in a 1:0.6 ratio with respect to gelatin (12 g MA) , as shown in Fig.2.1.a. The reaction was conducted at 40°C under continuous stirring for 4 hours. During the first 2 hours, the pH was readjusted to 9 every 15–20 minutes; in the following 2 hours, every 30–40 minutes. The basic pH favoured nucleophilic substitution by enhancing the reactivity of amino and hydroxyl groups.

4. **Dialysis:** The reaction mixture was transferred into dialysis membranes (MWCO 12–14 kDa) and dialysed against distilled water (neutral pH) at 200 rpm for 5 days. The water was replaced twice daily during the first two days, and once daily for the remaining three days. The experimental setup is showed in Fig. 2.1.b.

5. **Drying process:** The dialysed solution was freeze-dried using a ScanVac CoolSafe freeze dryer (LaboGene, Denmark) at - 40°C and approximately 0.5 Pa for one week, as shown in Fig. 2.1.c. The resulting product, a white porous sponge-like solid, was stored at room temperature (RT).

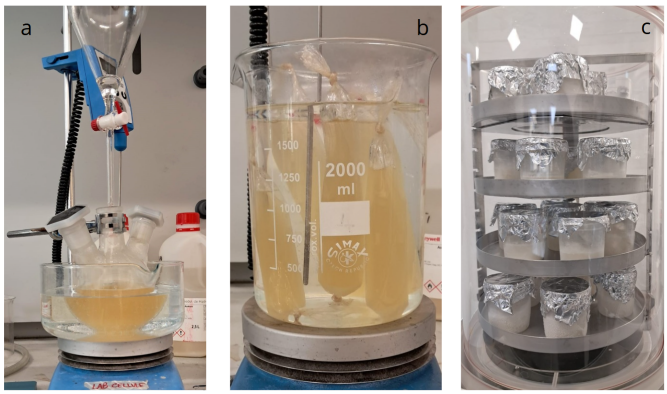

Figure 2.1: Photographic overview of GelMA synthesis and purification process.(**a**) Dropwise addition of methacrylic anhydride. (**b**) Dialysis process in distilled water. (**c**) Freeze-drying of dialysed GelMA using the ScanVac CoolSafe system.

2.1.2 Hydrogel synthesis

Following the synthesis of the base material, efforts were directed towards the development of a conductive GelMA-based hydrogel, optimised not only for stability, sensitivity, and conductivity, but also for its suitability in 3D printing processes. A key objective of this thesis was to enhance the mechanical and rheological properties of the formulation to yield a printable ink suitable for wearable sensor fabrication.

To address the issue of water evaporation, one of the principal limitations associated with the use of hydrogels in prolonged operational environments, water was partially replaced with a non-volatile, biocompatible solvent. Glycerol was selected for this purpose due to its well-documented cytocompatibility and low toxicity. Glycerol ($C_3H_8O_3$) is a viscous, transparent organic compound with three hydroxyl (-OH) groups, widely employed in biomedical applications. However, due to its limited ability to solubilize GelMA, resultin from an insufficient interaction with the polymer's methacryloyl and other functional groups, glycerol alone proved inadequate. Consequently, it was necessary to incorporate water to enable the initial dissolution of GelMA.

The solubilization process began with the preparation of a GelMA solution in water, intended to serve as a functional base for subsequent formulation tests. This was obtained using a magnetic stirrer and a thermostatic bath maintained at 40°C

(increased to 50°C where necessary) to prevent denaturation of the gelatin. GelMA was gradually added in increments of 10% w/v, resulting in a homogeneous solution up to a concentration of 100% w/v (Fig.2.2). Although the viscosity increased significantly at higher concentrations, the resulting solution remained processable and was adopted as a reference base for the development of water-glycerol mixtures.

Figure 2.2: Experimental setup used for GelMA-based hydrogel synthesis.

A series of hydrogel formulations were then prepared with varying water:glycerol ratios and GelMA concentrations in order to identify the optimal composition. The following combinations were evaluated:

- **1:4 (water:glycerol) with 20% w/v GelMA:** demonstrated acceptable handling properties, but the resulting hydrogels exhibited insufficient mechanical integrity;
- **1:4 with 15% and 10% w/v GelMA:** both concentrations produced gels that were excessively fragile and lacked cohesive strength;
- **1:2 with 33% w/v GelMA:** although mechanically robust, the hydrogel was overly rigid;
- **1:2 with 20% w/v GelMA:** provided the best compromise between viscosity, mechanical stability, and printability.

All formulations were characterised via uniaxial tensile and compression testing, as detailed in the *Results* section. Based on the comparative analysis, the

1:2 water:glycerol formulation with 20% w/v GelMA was selected as the optimal base composition. Subsequently, sodium chloride (NaCl) was incorporated as the electrolyte to impart ionic conductivity. NaCl was selected for its biocompatibility, availability, and low cost. Owing to its limited solubility in glycerol, the concentration was calculated based solely on the aqueous component of the formulation. Given the theoretical solubility of NaCl in water at room temperature (6.16 mol/L), and assuming one part water in a 1:2 water:glycerol ratio, a maximum feasible concentration of 1.232 mol/L was determined. A final concentration of 1 mol/L was chosen to ensure complete dissolution and functional performance. To further enhance the mechanical performance of the hydrogel, tannic acid was introduced prior to photoinitiator addition. A series of preliminary tests were conducted with tannic acid concentrations of 0.05%, 0.1%, 0.25%, 0.5%, 1%, and 2%, calculated as weight percentage (w/w) with respect to the total formulation mass. These formulations were evaluated by means of tensile testing. It was observed that concentrations exceeding 0.5% significantly increased the polymerisation time, with crosslinking kinetics generally slowing across all samples containing tannic acid. Nevertheless, the mechanical properties of the hydrogel were markedly improved in comparison to the tannic acid-free formulation—an outcome that will be further discussed in the *Results* section. Among the tested concentrations, 0.25% tannic acid was selected as the most suitable compromise, as it provided a significant enhancement in mechanical resistance to failure and a satisfactory elastic modulus, while preserving acceptable crosslinking times and good printability. The photoinitiator TPO (Triphenylphosphine Oxide) was incorporated into the formulation at a concentration of 2% w/w relative to the GelMA content. Upon UV irradiation, TPO decomposes to generate free radicals capable of initiating the polymerisation of methacrylate groups, thereby inducing the formation of a covalently crosslinked hydrogel network. The components and their respective quantities in the final formulation are summarised in Table 2.1.

Table 2.1: Summary of component quantities and calculation formulas.

Component	**Calculation Formula**
Water (mL)	Desired volume (e.g., 10 mL)
Glycerol (mL)	2 × water volume
Glycerol (g)	Glycerol volume × 1.26 g/mL
GelMA (g)	0.2 × (water + glycerol)
NaCl (g)	58.44 × water volume (L)
TPO (g)	2% of GelMA mass
TA (pure, g)	0.25% of total formulation mass
TA solution (g)	TA pure ÷ 0.4

For the specimens polymerized directly on a dog-bone-shaped PDMS mold, L360 stainless steel electrodes were inserted directly into the prepolymer solution at both ends before the photopolymerization began. This approach ensured the incorporation and mechanical integration of the electrodes into the hydrogel matrix during cross-linking. The entire assembly was then irradiated with UV light ($\lambda \approx 365\,\text{nm}$, intensity $\approx 36\,\text{mW/cm}^2$) for 3 minutes per side, using an Oriel Instruments model 97434-1000-1 UV lamp. This procedure allowed for complete polymerization of the hydrogel and stable encapsulation of the electrodes within the final sensor structure. The resulting hydrogel-based strain sensors were then ready for subsequent mechanical and electrical characterization. For the characterization of the 3D-printed samples, copper-coated polyimide film electrodes were used. These were placed at both ends of the sample, ensuring direct contact between the hydrogel and the exposed copper surface to allow electrical conduction.

2.2 Hydrogel and sensor characterization

2.2.1 Mechanical Characterisation

Tensile Test

The applied force (F) was measured by the load cell integrated into the movable grip. The test setup is illustrated in Fig. 2.3.

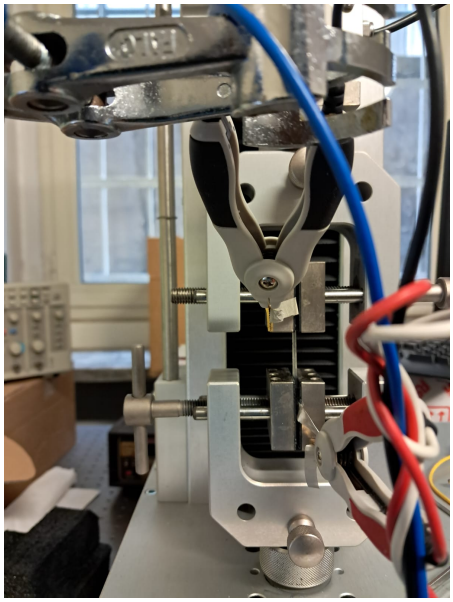

Figure 2.3: Tensile test setup

Measurements were recorded using the THSSD software (Gripsoft), which allows the user to input the sample's initial dimensions (length, width, and thickness). The engineering stress (σ) was calculated using the relation:

$$\sigma = \frac{F}{A}$$

where A is the cross-sectional area, obtained as the product of width and thickness. Prior to testing, the zero position was calibrated and the initial gauge length (l_0) of the sample was measured. The engineering strain (ε) was then computed as:

$$\varepsilon = \frac{l - l_0}{l_0}$$

with l representing the instantaneous displacement of the movable grip. Stress–strain curves were generated for all samples, and the Young's modulus was extracted from the slope of the linear elastic region. For each formulation, the modulus was calculated as the average value obtained from three or four independently tested samples to ensure statistical consistency and reproducibility. The tensile speed was set at 5 mm/min, and the following types of tests were performed:

1. **Breaking tests**: Samples were stretched until failure, enabling the determination of fracture stress and breaking strain.

2. **Durability tests**: Performed weekly, in which the samples were subjected to 20% strain of their initial length, to evaluate performance over time.

In addition to the tensile testing, a **bending test** was also performed to investigate the sensor's behaviour under flexural deformation. The experimental setup is shown in Fig. 2.4, where the sample is clamped at both ends and deflected by a central force applied through the upper jaw of the tensile testing machine.

To quantify the curvature induced during bending, a geometric approximation based on a right-angled triangle was used. Specifically, the bending angle α was calculated using the arctangent function:

$$\alpha = \arctan\left(\frac{\text{way}}{L_i}\right)$$

where *way* represents the vertical displacement applied at the centre of the sample, and L_i is the initial horizontal length between the clamping points.

Using the chord theorem, the radius of curvature R was calculated from:

$$\text{chord} = 2R \cdot \sin(\alpha) \quad \Rightarrow \quad R = \frac{\text{chord}}{2 \cdot \sin(\alpha)}$$

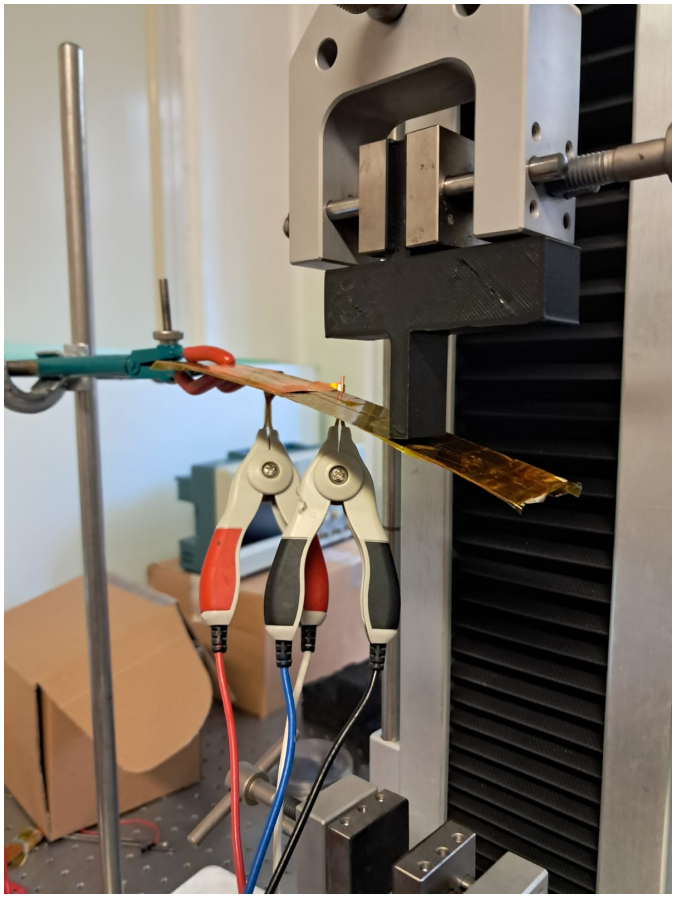

Figure 2.4: Bending test setup

Finally, the curvature k was obtained as the reciprocal of the radius:

$$k = \frac{1}{R}$$

These relations were used to assess the mechanical flexibility of the hydrogel sensor under cyclic bending.

2.2.2 Adhesion Test

To assess the adhesive properties of the sensor on different surfaces, an adhesion test was designed by photopolymerising the material directly onto microscope glass slides in contact with various substrates. For each trial, 20 g of the uncured hydrogel solution was deposited on the surface to be examined (Fig. 2.5.A) and subsequently cured under UV light while a test material was placed in contact with the hydrogel during polymerisation, thus simulating real bonding conditions under light exposure (Fig. 2.5.B).

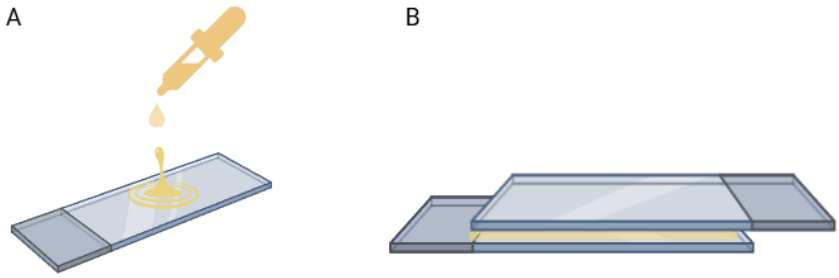

Figure 2.5: Schematic representation of the adhesion test procedure. A) Deposition of hydrogel precursor solution on surface. B) Substrate-hydrogel-glass system after exposure to UV light.

The selected substrates for this evaluation included glass, aluminium (with a polished surface finish) and untreated wood. These materials were chosen for their relevance in potential sensor packaging and interface scenarios, which offers a range of surface chemistries and roughness.

Following crosslinking, the adhesion force between the hydrogel and each substrate was quantified using the Z5 Single Column Tensile Machine. The test was carried out in tensile mode, applying a vertical displacement at a constant speed of 10 mm/s to pull the substrate away from the glass slide. The force required to detach each material from the hydrogel surface was recorded, allowing the evaluation of the adhesive strength. An example of the experimental setup for the adhesion test using a wood sample is shown in Fig. 2.6.

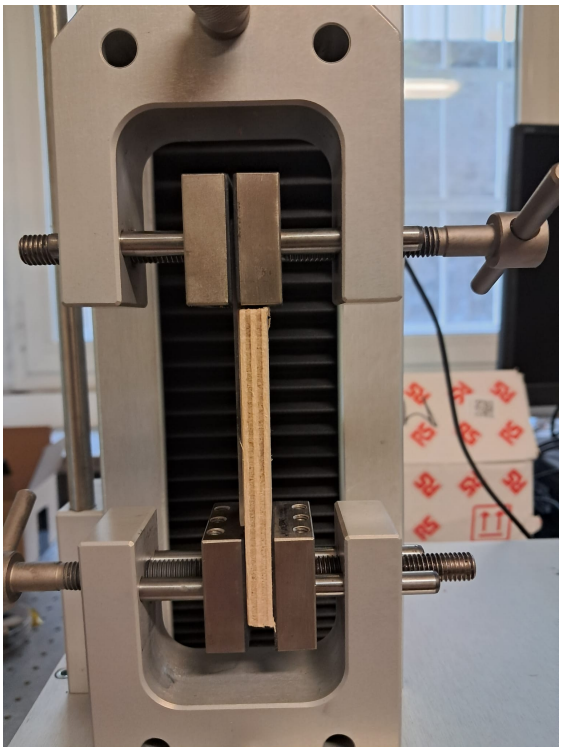

Figure 2.6: Experimental setup on the tensile testing machine for evaluating hydrogel adhesion to a wood substrate.

The results were used to qualitatively and quantitatively compare adhesion behaviours, identifying differences in interfacial bonding strength and failure modes (adhesive versus cohesive). This test provided comparative insights into the interfacial compatibility of the hydrogel with different surfaces, highlighting differences in bonding performance.

2.2.3 Electrical Characterisation

The electrical response of the sensor under mechanical strain was characterised using a BK Precision 894 LCR meter. Instrument control and data acquisition were managed via a custom LabVIEW interface (National Instruments). The measurement was conducted at a fixed frequency of 1000 Hz, and voltage amplitude at 1 V. This dual-voltage configuration was implemented to assess impedance variations under different excitation conditions.

The impedance of the sensor was modelled as a parallel combination of a resistor and a capacitor. An alternating voltage signal was employed to prevent charge accumulation and electrode polarisation, phenomena that can occur under direct current (DC) stimulation due to ion migration and the formation of electrical double layers. These effects can distort the electrical characteristics of the hydrogel and compromise the accuracy of the measurements.

Electrical measurements were performed concurrently with the tensile tests, enabling the monitoring of both resistance and capacitance in real time as a function of applied strain (Fig. 2.3). Sensor sensitivity was determined from the slope of the $\Delta R/R_0$ versus ε curve.

2.2.4 Rheological and Photocuring Characterisation

The rheological behavior and photo-crosslinking kinetics of the hydrogel formulations were comprehensively evaluated using an Anton Paar MCR302 Modular Compact Rheometer equipped with a H-PTD200 temperature-controlled measuring unit and a D-PP25 parallel plate geometry (25 mm diameter, 0.3 mm gap). These tests provided essential insights into the material's viscoelastic properties before and after crosslinking, as well as its suitability for UV-based photopolymerisation.

The characterization began with a flow test to measure the viscosity of the uncured hydrogel as a function of shear rate.This analysis was instrumental in assessing the printability of the hydrogel and its behavior under mechanical stress during layer deposition.

Subsequently, a amplitude sweep tests was performed in the uncured (liquid-like) and cured (solid-like) states of the hydrogel. The purpose of these tests was to define the viscoelastic region (LVR), within which the material's structure responds elastically to small deformations without undergoing damage or nonlinear

behavior. In the pregelled solution, the sweep helped verify the viscoelastic nature of the system and allowed selection of appropriate parameters for subsequent tests. In the gel state, the test provided information about the structural rigidity and deformation limits.

Finally, a photorheology test was carried out to monitor the crosslinking kinetics of the material under UV irradiation in real time. The rheometer was coupled to a UV light source (385 nm) via an optical fiber system. The test was performed in oscillatory mode at a fixed frequency of 10 Hz and strain amplitude of 1%. After a stabilization delay of 30s, the sample was irradiated continuously while the evolution of the storage modulus (G') and loss modulus (G'') was recorded at regular intervals. The crossover point between G' and G'' indicated the gelation time, while the subsequent plateau of G' reflected the extent of crosslinking. This methodology allowed comparison between different formulations in terms of polymerization rate and final mechanical properties.

All rheological measurements were conducted at a controlled temperature of 25 °C. The resulting data were used to support material selection and optimization, ensuring that the printed sensors exhibit appropriate mechanical stability, viscoelasticity, and responsiveness to UV curing.

2.3 Hydrogel and sensor printing

The printing of hydrogel-based strain sensors was performed using a digital light processing (DLP) 3D printer, the Asiga UV MAX X (UV385). This printer operates via DLP imaging with Active Layer Monitoring (SPS™) technology, offering high-precision polymerisation through projection of structured UV light. The system features an auto-calibrating LED source at 385 nm (with optional 365 nm and 405 nm wavelengths), and provides a pixel resolution of 27 μm, suitable for high-resolution microstructure fabrication. The build volume of the UV MAX X is 51.8 $\times$ 29.2 $\times$ 75 mm.

Printing files were prepared using Asiga Composer, the proprietary slicing software included with the system. Sensor geometries designed in CAD were imported as .stl files and converted into printable layers. Process parameters such as exposure time, layer thickness, and light intensity were defined within the software interface before initiating the print job. The printer was connected via Ethernet and operated under ambient temperature and humidity conditions. After fabrication, the printed structures were post-processed to remove uncured resin and stabilised via UV post-curing. Fig. 2.7.A shows the visualisation of the selected sensor structures in the layer-by-layer preview generated by Asiga Composer. During the printing process, real-time monitoring of layer thickness and alignment was performed via the integrated front panel interface, as shown in

Fig. 2.7.B.

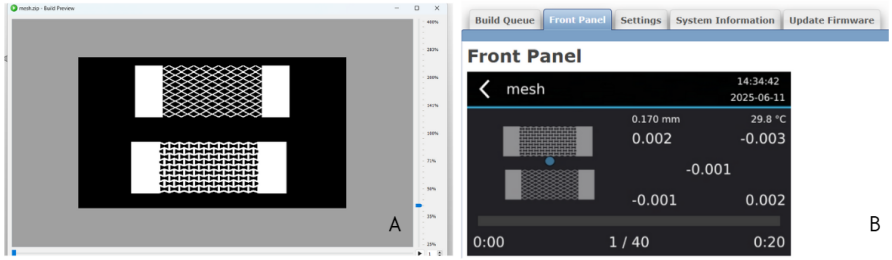

Figure 2.7: Printing of hydrogel-based mesh strain sensors using the Asiga UV MAX X. (A) Layer-by-layer build preview generated in Asiga Composer, showing two different mesh geometries. (B) Real-time interface of the printer during fabrication, displaying layer thickness (170 μm), internal temperature, and printing progress.

Chapter 3

Results and Discussion

3.1 Sensor optimization and characterization

Three different GelMA hydrogel formulations – 33% 1:2, 20% 1:4, and 20% 1:2 (w/v) – were tested to evaluate their suitability as strain-responsive materials for wearable applications. These compositions were selected to explore how variations in polymer concentration and dilution ratio influence both mechanical and electrical performance.

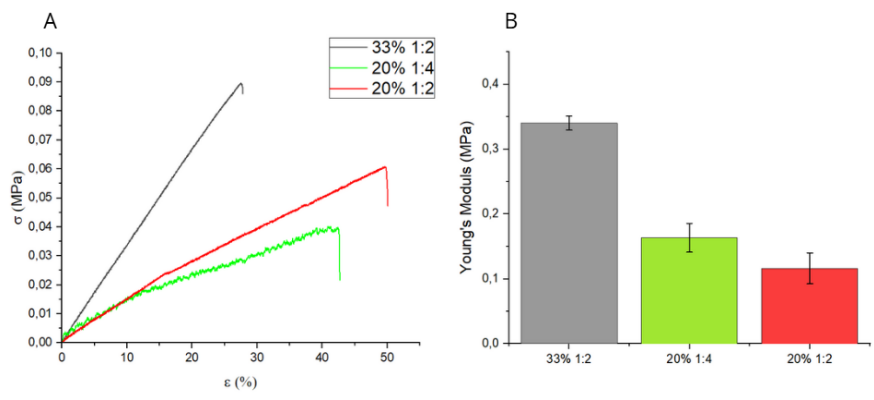

Figure 3.1: (A) Stress-strain curves for the three GelMA hydrogel formulations (B) Comparison of Young's modulus (mean ± SD, $n = 4$)

Uniaxial tensile tests were performed on dog-bone-shaped printed specimens to characterise their stress–strain behaviour and determine Young's modulus. As shown in Fig. 3.1A, the 30% 1:2 formulation exhibited the highest stress response under tensile loading, consistent with its elevated polymer content. The corresponding Young's modulus, extracted from the linear elastic region of the curve, was on average 0.34 MPa (Fig. 3.1B), based on four replicate samples. In

comparison, the 20% 1:4 and 20% 1:2 formulations displayed reduced stiffness, with average moduli of 0.17 MPa and 0.13 MPa, respectively (n = 4). These values reflect the looser polymer network and reduced crosslinking degree at lower GelMA concentrations.

In addition to stiffness, elongation at break also varied with composition: the 20% 1:2 samples reached nearly 50% strain at rupture, indicating higher flexibility. This mechanical compliance is advantageous for wearable devices, which must accommodate dynamic movements without failure.

Electrical performance was evaluated by recording the relative resistance change ($\Delta R/R$) during deformation. As shown in Fig. 3.2.A, the 20% 1:2 formulation showed the most pronounced change, with $\Delta R/R$ approaching 45% at 50% strain. In contrast, the 30% 1:2 and 20% 1:4 samples exhibited more modest variations in resistance.

The sensitivity, calculated as the slope of the $\Delta R/R$ vs. strain curve, is summarised in Fig. 3.2.B. The 20% 1:2 samples achieved the highest mean sensitivity of 0.85 (n = 4), outperforming both 20% 1:4 (0.67) and 30% 1:2 (0.52). These results suggest that a lower crosslinking density, associated with reduced stiffness, enhances ionic mobility and thus improves the electromechanical coupling efficiency.

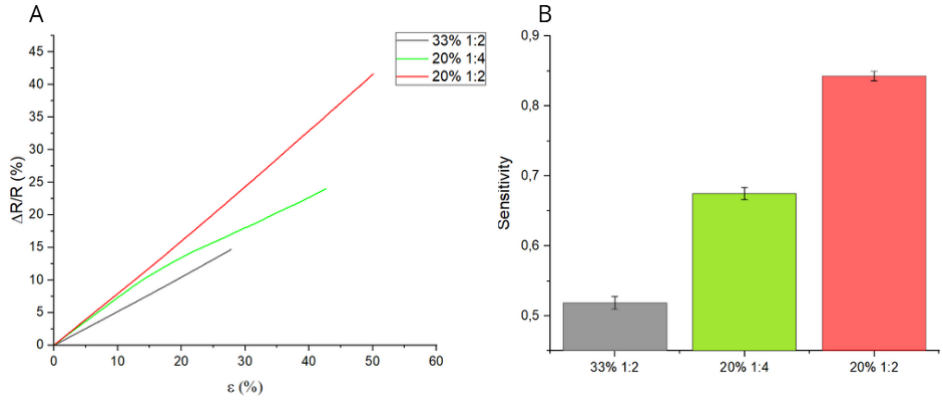

Figure 3.2: (A) Change in relative resistance as a function of applied strain for the three hydrogel formulations. (B) Sensitivity values calculated from the slope of the corresponding $\Delta R/R$ versus strain curves (mean ± SD, $n = 4$).

In light of the results, the 20% 1:2 formulation was selected for subsequent sensor fabrication. It presents an optimal balance between sufficient mechanical integrity and enhanced electrical responsiveness, meeting the functional criteria required for high-performance, flexible, and biocompatible strain sensors.

3.1.1 Citric Acid

To further optimise the performance of the selected 20% GelMA 1:2 formulation, additional tests were conducted by incorporating citric acid (CA), a multifunctional organic acid known for its ability to participate in secondary cross-linking interactions. Citric acid contains carboxylic and hydroxyl groups capable of forming hydrogen bonds or ionic interactions with the gelatin backbone or the surrounding aqueous environment. This characteristic made it a suitable candidate to potentially enhance the mechanical integrity and structural stability of the hydrogel.

Different concentrations of citric acid were tested and labelled as 00CA, 20CA, 30CA, and 50CA, where "XXCA" denotes a formulation containing XX% CA by weight with respect to the amount of GelMA (w/w). For instance, 20CA corresponds to 20 mg of citric acid per 100 mg of GelMA in the formulation.

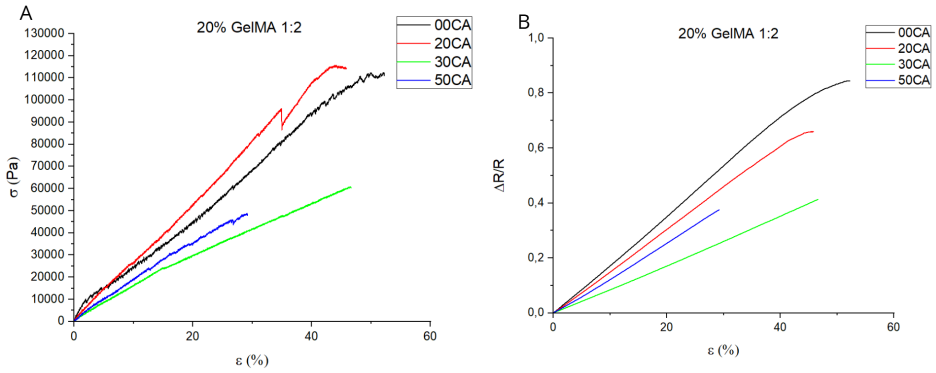

Figure 3.3: (A)Stress–strain curves of 20% GelMA 1:2 formulations with different citric acid contents. (B) Relative resistance change as a function of applied strain for the same samples.

The stress–strain behaviour of these modified hydrogels is shown in Fig. 3.3A. Among the tested formulations, 20CA displayed a modest increase in maximum stress compared to the reference (00CA), suggesting a minor reinforcement effect. However, no significant improvement was observed in terms of elastic modulus or strain at break. Concurrently, electrical measurements under deformation (Fig. 3.3B) showed a progressive decline in resistance variation with increasing citric acid content, indicating a reduced electromechanical responsiveness.

To quantitatively assess these effects, the Young's modulus and strain sensitivity were calculated and are reported in Fig. 3.4. The modulus values (Fig. 3.4A) remained relatively unchanged across the different CA concentrations, with minor variations within experimental uncertainty. In contrast, sensitivity (Fig. 3.4B), decreased from 0.84 in the unmodified sample (00CA) to 0.66 in the 50CA condition.

Overall, these results indicate that the incorporation of citric acid does not lead to appreciable improvement in mechanical or electrical performance. On the contrary, higher concentrations appear to reduce the strain sensitivity, possibly due to increased ionic screening or hindered charge mobility in the more densely packed hydrogel matrix. Consequently, citric acid was not selected for further sensor development.

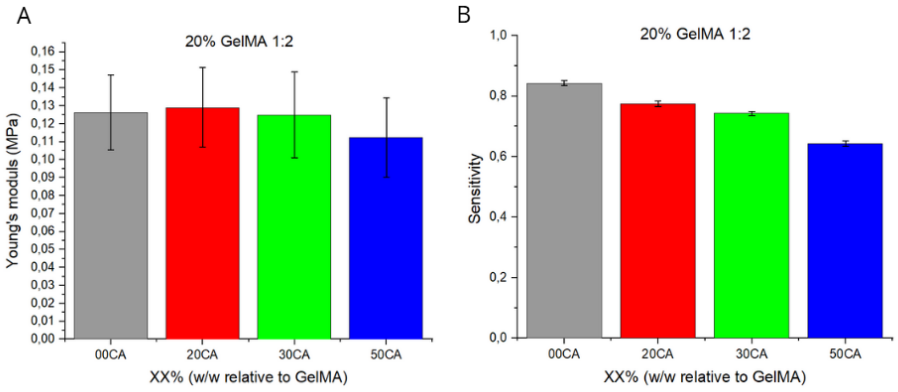

Figure 3.4: (A)Young's modulus for samples containing increasing citric acid concentrations. (B) Corresponding sensitivity values (mean ± SD, $n = 3$).

3.1.2 Tannic Acid

Tannic acid (TA), due to its high density of phenolic hydroxyl groups, is able to form multiple hydrogen bonds and coordination interactions with polymer chains, making it a promising additive to improve both the mechanical strength and adhesive performance of hydrogels. As previously mentioned, its incorporation can potentially lead to secondary crosslinking, increased toughness, and increased stability of the polymer network.

To explore the potential of tannic acid (TA) as an additive to improve the properties of hydrogels, an initial approach was based on the post-fabrication immersion of pre-crosslinked GelMA samples in aqueous TA solutions. This method, previously employed in hydrogel systems to introduce physical reinforcement and interpenetrating interactions [50], was tested on 20% 1:2 GelMA samples. The aim was to evaluate whether such treatment could further improve the mechanical and electromechanical performance of the constructs.

Dog bone-shaped samples were immersed in a 5% (w/v) aqueous solution of tannic acid and extracted at different time intervals (30 min, 1 h, 9 h and 15 h), as shown in Fig. 3.5A. However, significant undesirable effects were observed.

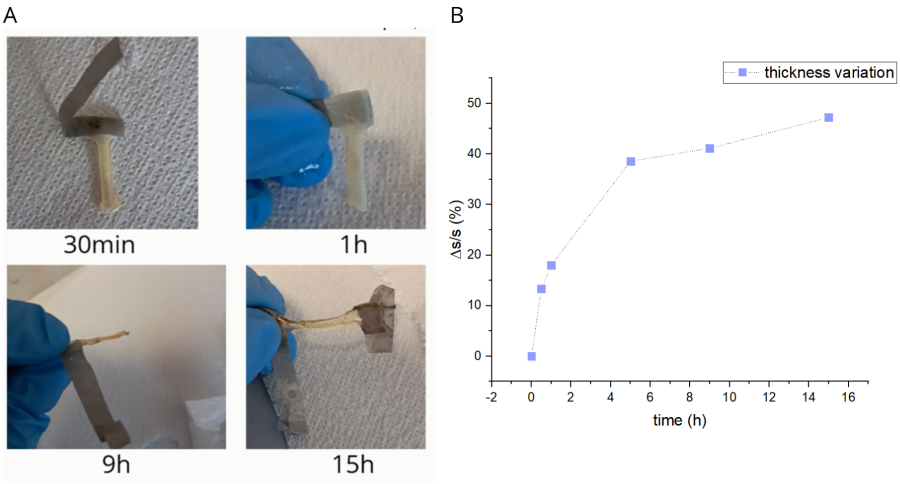

Figure 3.5: (A) Representative images of 20% GelMA 1:2 hydrogel samples immersed in 5% tannic acid solution and extracted after different times. (B) Relative thickness variation ($\Delta s/s$) as a function of immersion time.

The immersion led to a pronounced stiffening and brittleness of the hydrogels. The samples became opaque, brittle and, in some cases, spontaneously fractured during handling. These macroscopic alterations were accompanied by a substantial reduction in thickness (up to 45%), as reported in Fig. 3.5B. The volume loss is attributed to the expulsion of glycerol and the dehydration of the polymer network, probably promoted by the strong intermolecular interactions induced by TA.

Due to these severe structural alterations, it was not possible to perform tensile tests on the treated samples.

Given the unsatisfactory outcome of the immersion approach, a second strategy was explored, whereby tannic acid (TA) was incorporated directly into the hydrogel formulation prior to photopolymerisation. This method allowed for a more homogeneous distribution of TA throughout the polymer matrix, potentially facilitating stable interactions with the GelMA network while preserving the integrity and printability of the material.

TA was first dissolved in distilled water at a fixed ratio of 2:3 (w/w), meaning two parts of tannic acid for every three parts of water. The base composition consisted of 20% w/v GelMA (20 mg GelMA per 1 mL total solution), with a 1:2 volumetric ratio of water to glycerol, and 1 M NaCl added to confer ionic conductivity. TPO was included at 2% w/w with respect to GelMA to ensure efficient UV-induced crosslinking.

Using this formulation, a series of samples was prepared by varying the tannic acid concentration relative to the total solution volume. The concentrations tested were 0%, 0.05%, 0.1%, 0.25%, 0.5%, 1%, and 2% v/v TA. These are hereafter referred to as "n TA" samples, where "n" denotes the percentage of TA added.

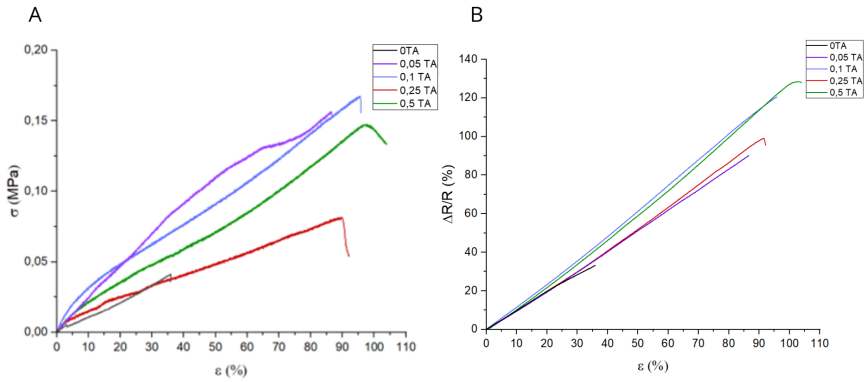

Figure 3.6: (A) Stress–strain curves of hydrogel formulations with increasing tannic acid content. (B) Relative resistance variation for each TA-modified sample.

As shown in Fig. 3.6, the addition of TA influenced the mechanical response under tensile loading. All samples were subjected to uniaxial tensile tests to assess

elasticity, strain at break, and resistance variation under deformation. The data indicate a significant enhancement in mechanical performance up to 0.25% TA, beyond which samples exhibited diminished flexibility and increased polymerisation times. A substantial improvement in elongation at break is observed across all formulations containing TA, as shown in Fig. 3.7. The incorporation of even low concentrations of TA led to a marked increase in stretchability, with all TA-containing samples exhibiting significantly higher failure strains compared to the TA-free hydrogel (>85%)).

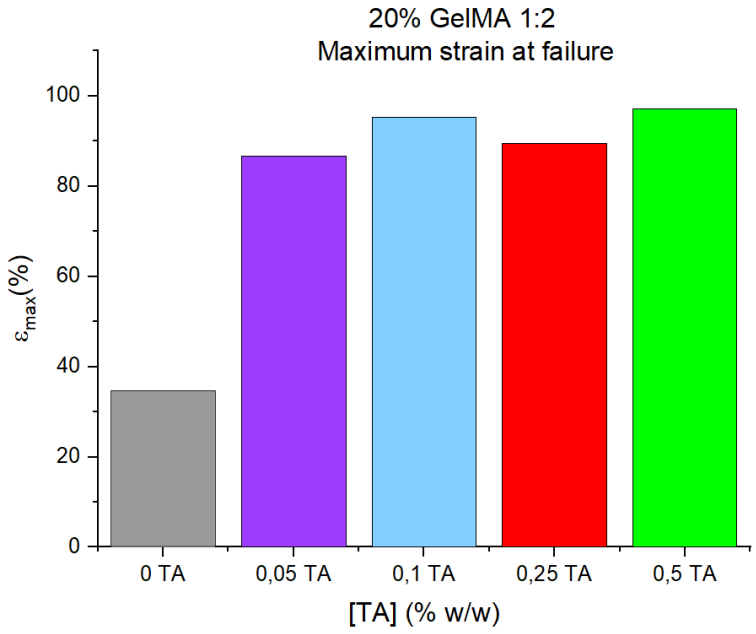

Figure 3.7: Maximum strain at break for formulations with increasing tannic acid content.

Finally, Fig. 3.8 compares the average Young's modulus (A) and strain sensitivity (B) for the various GelMA hydrogel formulations incorporating different concentrations of tannic acid (TA).Improvement in mechanical stiffness with the addition of TA is confirmed, with the Young's modulus reaching a peak at 0.1% w/w. However, at higher concentrations, such as 0.25% and 0.5%, the modulus slightly decreased, likely due to changes in network organisation or excessive plasticisation effects introduced by the phenolic additive.

In terms of sensing performance, all TA-containing samples showed a notable increase in strain sensitivity compared to the control (0% TA), with values stabilising above 1.2. This improvement reflects the enhanced interfacial adhesion and more homogeneous conductive network achieved through the presence of TA, which supports consistent resistance changes during deformation.

Among the tested formulations, the hydrogel containing 0.25% TA emerged as the most effective compromise. Although not the absolute best in either mechanical stiffness or sensitivity, it provided sufficiently high values for both parameters, while also maintaining excellent printability and favourable crosslinking behaviour. Its balanced performance across mechanical, electrical, and processing domains led to its selection as the optimised composition for subsequent sensor fabrication and testing.

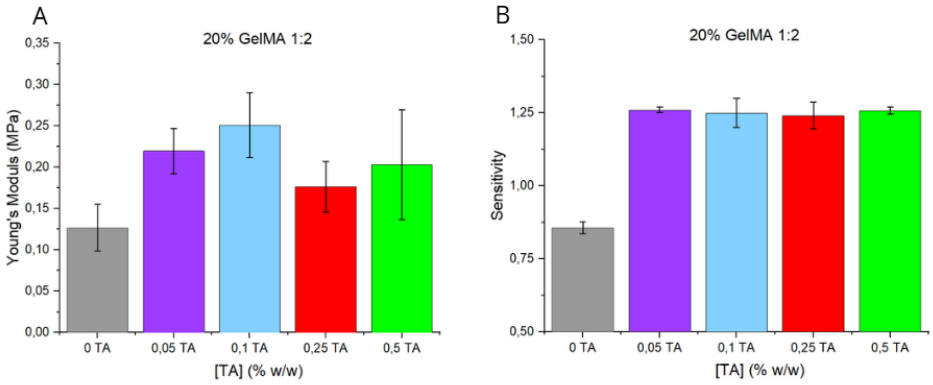

Figure 3.8: (A) Average Young's modulus; (B) Strain sensitivity of each TA formulation (mean ± SD, $n = 3$).

Durability Test

To evaluate the long-term stability of the hydrogel-based strain sensors, a durability test was performed over a period of 70 days. Two sets of samples were compared: one based on the standard 20% GelMA 1:2 formulation without additives, and the other incorporating 0.25% (w/w) tannic acid. All samples were subjected to periodic mechanical-electrical characterization by applying a constant strain of 20%, and the Young's modulus and strain sensitivity were extracted accordingly.

Importantly, the specimens were stored in standard Petri dishes without sealing or environmental control, in order to realistically simulate the response of the material under ambient fluctuations in temperature and humidity.

As shown in Fig. 3.9, the Young's modulus (panel A) exhibited moderate fluctuations over time for both formulations, likely due to progressive water loss and plasticizer migration. However, no drastic degradation was observed in either condition. The TA-containing samples retained mechanical integrity comparable to or slightly better than the control, even after 70 days.

More significantly, the electrical response (Fig. 3.9B) demonstrated improved stability in the presence of tannic acid. The sensitivity remained consistently higher

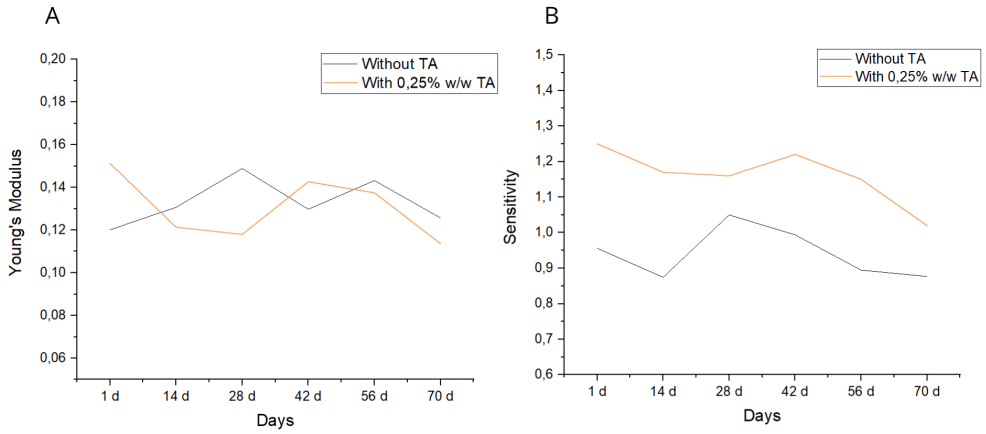

Figure 3.9: (A) Young's modulus of GelMA-based hydrogel samples with and without 0.25% w/w tannic acid (TA), evaluated after fixed storage intervals. (B) Corresponding evolution of strain sensitivity

across all timepoints compared to the control group, with a smaller decline in performance over time. This supports the hypothesis that TA promotes network reinforcement and reduces the susceptibility of the hydrogel to environmental stress, contributing to longer-lasting strain-sensing capability.

These results confirm that the inclusion of 0.25% TA not only enhances initial mechanical and electrical performance, but also positively impacts the operational lifespan of the sensors under ambient storage conditions.

Bending Test

To investigate the piezoresistive behaviour of the hydrogel-based strain sensors under flexural deformation, bending tests were performed on three independently fabricated samples. The relative resistance change ($\Delta R/R$) was plotted against the curvature, expressed as the reciprocal of the radius ($1/R$).

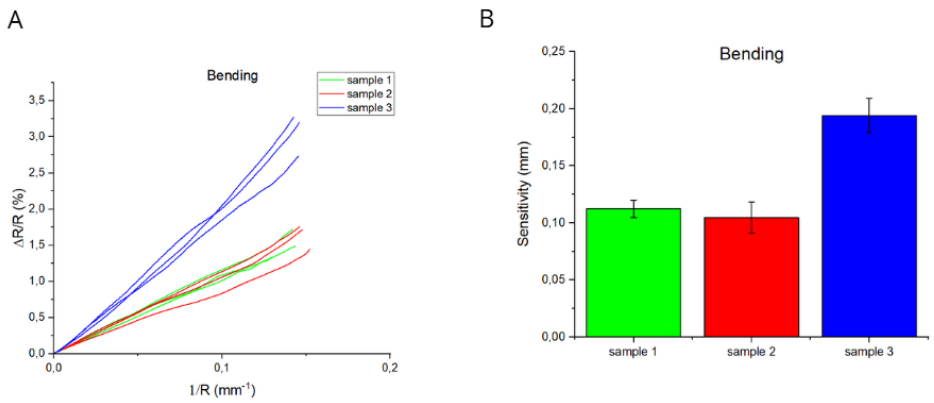

Figure 3.10: (A) Relative resistance variation ($\Delta R/R$) as a function of curvature ($1/R$) for three hydrogel-based strain sensors subjected to bending. (B) Sensitivity values extracted as the slope of the corresponding curves in panel A, expressed in mm. Error bars indicate standard deviation (n=3).

As shown in Fig. 3.10A, all three tested samples exhibited a clear increase in relative resistance with increasing curvature, confirming the piezoresistive nature of the sensors under bending deformation. Samples 1 and 2 (green and red curves, respectively) displayed nearly identical behaviours, with moderately linear responses up to $1/R \approx 0.15\,\mathrm{mm}^{-1}$ and maximum $\Delta R/R$ values ranging from approximately 1.4% to 1.6%. In contrast, sample 3 (blue curve) demonstrated a significantly steeper slope, reaching a relative resistance change exceeding 3.0% at the same curvature value.

The corresponding sensitivity values, calculated as the slope of the $\Delta R/R$ versus $1/R$ curves, are reported in Fig. 3.10B. Consistent with the trend observed in panel A, sample 3 exhibited the highest sensitivity (approximately 0.20 mm), while samples 1 and 2 showed comparable and lower values around 0.12 mm. This variability may arise from minor differences in hydrogel deposition, electrode contact uniformity, or internal ionic distribution across the polymer matrix.

Such variation among samples may arise from slight differences in hydrogel deposition, electrode contact uniformity, or internal conductivity distribution within the polymer network. Nonetheless, the consistent linear trend across all replicates confirms the repeatability and reliability of the sensor response.

Overall, these results demonstrate that the developed hydrogel sensor maintains effective sensing capability under flexural deformation, suggesting its applicability in complex mechanical environments, such as wearable systems or curved surface interfaces.

Adhesion Test

To evaluate the adhesive performance of the developed hydrogel sensors, adhesion tests were conducted across various substrates and compositions, focusing particularly on the role of tannic acid (TA) in enhancing interfacial bonding. The results are presented in Fig. 3.11 and Fig. 3.12.

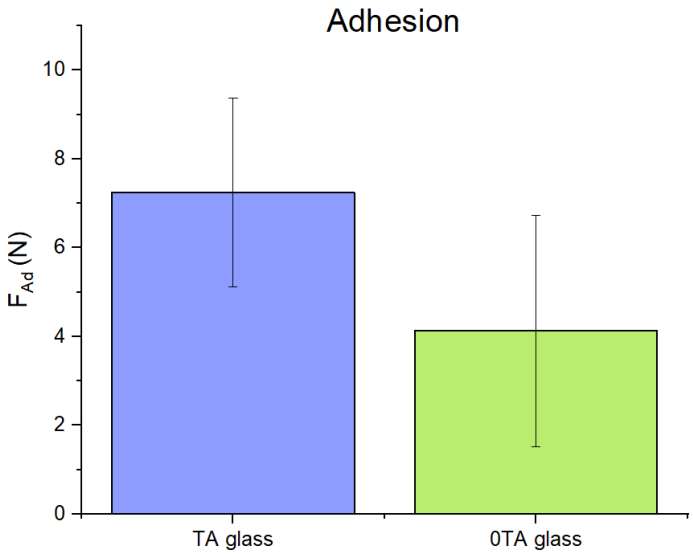

Figure 3.11: Comparison of adhesion force between hydrogel and glass substrates with and without TA addition.

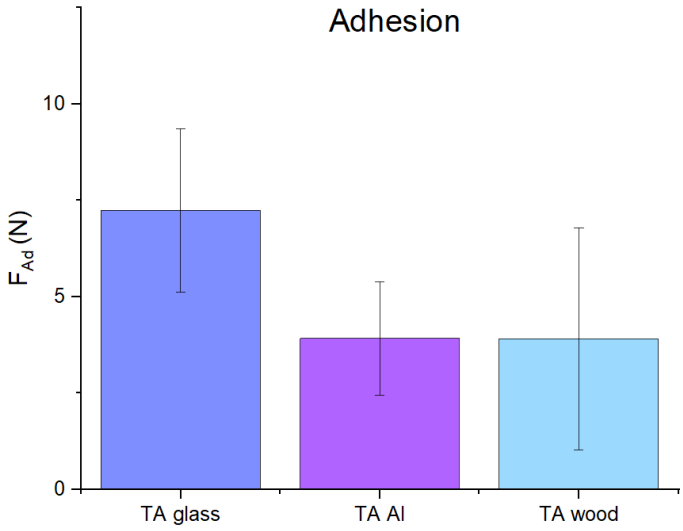

Figure 3.12: Adhesion force of TA-containing hydrogels across different substrates: glass, aluminium, and wood.

As shown in Fig. 3.11, the introduction of tannic acid into the hydrogel formulation significantly enhanced adhesion to glass surfaces. The average detachment force increased from approximately 4.1 N for the control sample (without TA) to around 7.2 N with 0.25% w/w TA, demonstrating the polyphenol's ability to promote stronger surface interactions, likely through hydrogen bonding and π–π stacking.

To further investigate substrate-dependent behaviour, tests were also conducted on aluminium and untreated wood samples using the TA-based formulation (Fig. 3.12). While the adhesive force on glass remained the highest, reaching nearly 7.5 N, reduced adhesion was observed on aluminium and wood, averaging approximately 3.4 N. This suggests that while TA promotes adhesion on smooth and chemically favourable surfaces like glass, its effect is more limited on rougher or less polar substrates.

These findings confirm the dual benefit of tannic acid in enhancing hydrogel adhesion and demonstrate its relevance for substrate-dependent applications. Notably, all samples exhibited adhesive failure at the interface rather than cohesive rupture within the hydrogel matrix, indicating good bulk integrity and reliable interfacial measurements.

3.1.3 Photorheological characterisation

The photorheological analysis was conducted to investigate the influence of tannic acid (TA) on the flow behaviour of GelMA-based prepolymer solutions. Understanding the rheological response is essential not only for optimising 3D printing parameters but also for predicting how TA concentrations may affect print fidelity and resolution. Viscosity measurements were carried out under controlled temperature conditions across a broad range of shear rates to assess shear-thinning behaviour, which is critical for extrusion-based processes.Fig. 3.13 shows the viscosity profiles of GelMA-based prepolymer formulations containing increasing concentrations of TA (0.05%, 0.1%, 0.25% and 0.5% w/w) as a function of the shear rate. All tested solutions exhibited a shear-thinning trend, where viscosity decreased with increasing shear rate, a behaviour typical of polymeric fluids.. The addition of TA had a clear impact on viscosity values: higher concentrations led to a general increase in viscosity over the entire shear rate range, likely due to the formation of hydrogen bonds and physical entanglements between polyphenolic groups of TA and the gelatin chains.

Among the formulations, the 0.5% TA sample showed the highest initial viscosity (approximately 10.5 Pa·s at low shear rates), maintaining elevated values even under high shear. Conversely, the 0.05% TA sample displayed the lowest viscosity, with values starting below 6.5 Pa·s and dropping more rapidly. These results suggest that TA not only modulates the mechanical behaviour of the final hydrogel but also

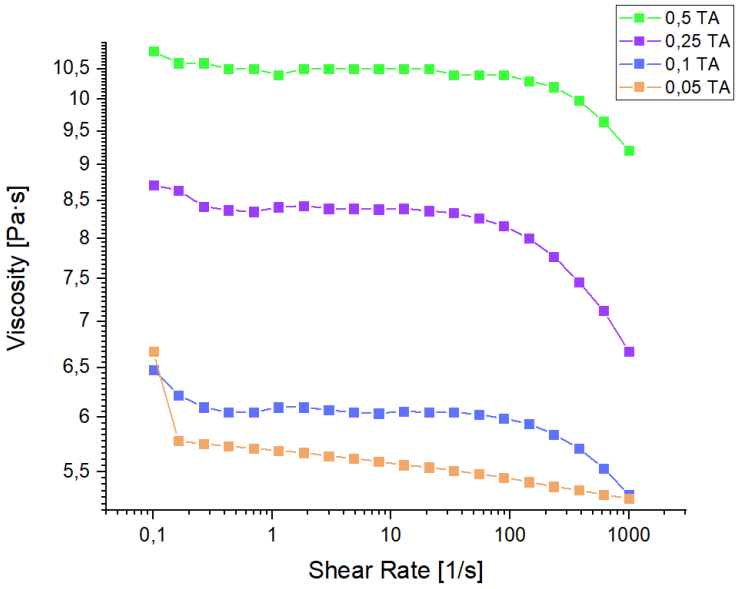

Figure 3.13: Viscosity curves plotted as a function of shear rate in logarithmic scale.

significantly alters the flow dynamics of the precursor, influencing its printability. An intermediate behaviour was observed at 0.25% TA, which represents a suitable compromise between manageable viscosity and functional reinforcement, as further discussed in the mechanical testing section.

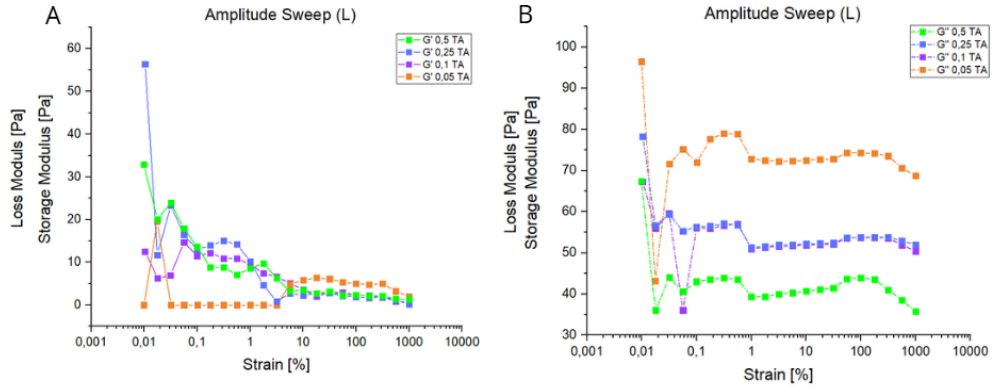

Figure 3.14: Amplitude sweep test (liquid state). A) Storage modulus G' and B)Loss modulus G'' plotted as a function of strain (%).

The amplitude sweep test in liquid state was performed to evaluate the viscoelastic response of the precursor solutions at varying TA concentrations prior to UV crosslinking. Specifically, the storage modulus G' Fig. 3.14.A and loss modulus G'' Fig. 3.14.B were measured over a strain range from 0.01% to 10% at a constant angular frequency of 1 Hz. This preliminary characterisation was essential to identify the linear viscoelastic region (LVR) of each formulation, thus determining the appropriate strain amplitude to be employed in the subsequent photorheological analysis.

As shown in Fig. 3.14, all samples exhibited relatively stable G' and G'' values at low strain amplitudes, followed by a drop outside the LVR, which is indicative of the disruption of internal structure under larger deformations. Increasing the concentration of TA resulted in higher values of both G' and G'', reflecting enhanced elastic and viscous contributions to the mechanical response. The formulation containing 0.05% w/w TA showed the highest G'' across the strain range, pointing to a predominance of viscous behaviour, whereas the 0.25% and 0.5% TA samples exhibited significantly higher G' values, suggesting the formation of more structured networks even in the uncured state.

The identification of the LVR from this test enabled the selection of an optimal strain amplitude—within the range of structural linearity—for accurate monitoring of modulus evolution during UV curing.

Photopolymerisation kinetics of the hydrogel formulations were investigated via photorheology under oscillatory shear conditions at a fixed frequency of 1 Hz and

a strain amplitude of 1%, within the linear viscoelastic region as determined by preliminary amplitude sweep tests. Fig. 3.15 shows the evolution of the storage modulus (G') and loss modulus (G'') as a function of time for different concentrations of tannic acid (TA), highlighting the gelation behaviour before and after UV light exposure.

The shaded region (0–30 s) corresponds to the dark phase prior to UV illumination, during which all samples exhibited low and stable viscoelastic moduli, indicative of a predominantly viscous, liquid-like state. Upon activation of the light source at $t = 30$ s, a rapid increase in G' and G'' was observed, marking the onset of network formation due to photoinitiated crosslinking.

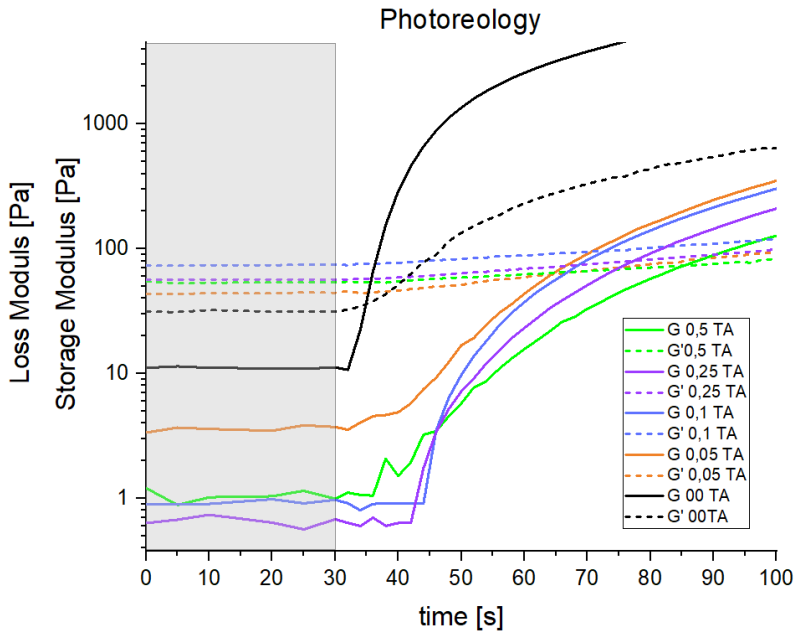

Figure 3.15: Photorheological analysis of hydrogels with varying TA concentrations. UV exposure (initiated at 30 s, grey region) triggered crosslinking, with higher TA contents delaying gelation and enhancing final stiffness.

The gelation behaviour of the formulations is summarised in Table 3.1. A distinct gelation point, defined by the crossover of G' and G'', was identified for all samples. The control sample without TA exhibited a rapid gelation occurring within 4.5 seconds from the onset of irradiation. As shown in Table 3.1, the incorporation of tannic acid (TA) significantly influenced the gelation kinetics. Even at a low concentration of 0.05% w/w, the gelation time increased markedly to 34.4 seconds. Further increments in TA content progressively delayed the gelation point.

This trend confirms that the addition of TA not only modulates the final stiffness

Table 3.1: Gelation time for different formulations containing tannic acid (TA). The gelation point was determined as the crossover between G' and G'', excluding the lamp activation delay.

[TA] (% w/w)	Gelation time (s)
0	4.5
0.05	34.4
0.1	43.2
0.25	47.4
0.5	55.1

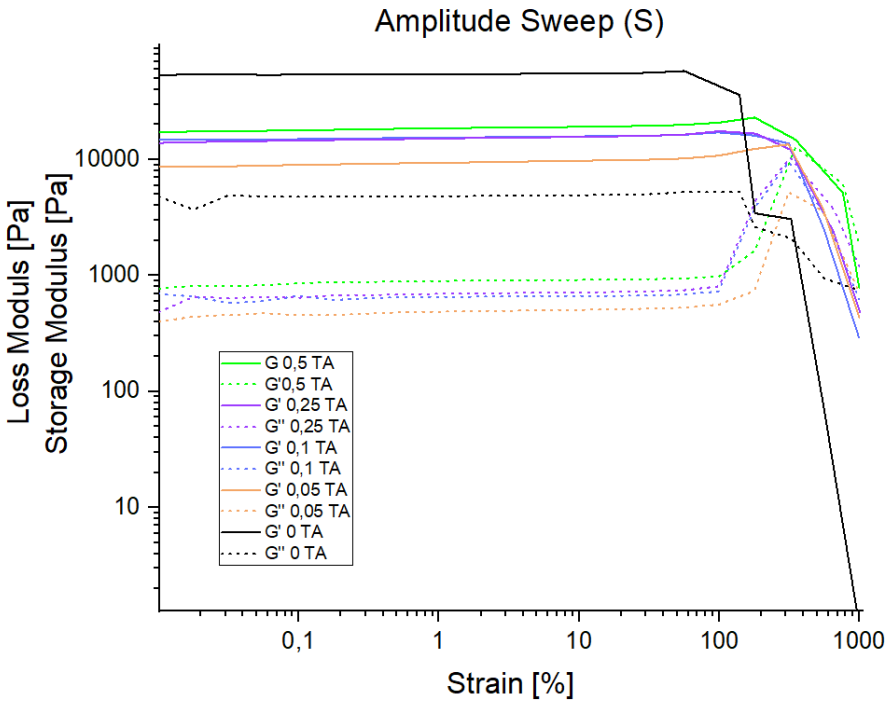

Figure 3.16: Amplitude sweep in the solid state. Storage modulus (G') and loss modulus (G'') of hydrogels with different TA contents as a function of applied strain.

of the network but also slows the crosslinking kinetics. Higher concentrations of TA led to prolonged gelation times, likely due to steric hindrance and competitive hydrogen bonding interactions that reduce the availability of reactive methacrylate groups. These observations are in agreement with preliminary trials, in which formulations with TA concentrations above 0.5% w/w exhibited excessively slow photopolymerisation, making them unsuitable for rapid curing processes. Despite the delayed gelation, the final storage modulus (G') increased with TA content, indicating an enhancement in the mechanical robustness of the network. This stiffening effect can be attributed to secondary physical interactions, such as hydrogen bonding and π–π stacking, formed between TA molecules and the gelatin backbone, which act synergistically with the primary covalent crosslinks. These findings highlight the dual and tunable role of TA in influencing both the gelation dynamics and the final mechanical integrity of the hydrogel, providing a critical design parameter for optimising hydrogel-based strain sensors in terms of printability and stability.

To evaluate the mechanical robustness of the photocrosslinked hydrogels under increasing deformation, a strain sweep test was performed on solid samples. Figure 3.16 shows the evolution of the storage modulus (G') and loss modulus (G'') as a function of strain amplitude, with values spanning from 0.05% to 1000% in a logarithmic scale.

All formulations exhibited a relatively broad linear viscoelastic region (LVR), where both G' and G'' remained constant. The extent of the LVR increased slightly with the concentration of tannic acid (TA), indicating improved mechanical resilience. The critical strain, defined as the point where G' starts to deviate significantly from its initial plateau, shifted to higher strain values with increasing TA content, suggesting enhanced elasticity and network stability.

Moreover, G' consistently exceeded G'' in all tested samples, confirming a predominantly elastic behaviour throughout most of the strain range. The hydrogel without TA showed the lowest stiffness and a narrower LVR, supporting previous photorheological results. In contrast, the sample with 0.5% TA displayed the highest storage modulus and preserved its elastic regime over a wider strain interval, highlighting the reinforcing effect of TA crosslinking.

3.1.4 Material tests

To evaluate the photo-curing behaviour of the hydrogel precursors and guide the selection of optimal parameters for DLP printing, preliminary curing tests were conducted. These experiments aimed to correlate the exposure energy, expressed as $E = I \cdot t$ (in mJ/cm^2 or mJ/mm^2), with the final cured dimensions of hydrogel structures, both in terms of layer thickness and lateral resolution (diameter). Two distinct formulations were investigated: one without tannic acid (TA), and

one containing 0.25% TA, allowing for a comparative analysis of TA's effect on photopolymerisation.

In the first set of tests, a TA-free formulation containing the yellow dye tartrazine was examined to evaluate the curing behaviour in the absence of UV-absorbing species. The exposure energy was modulated by varying the exposure time at fixed light intensities of 20, 30, and 40 mW/cm^2. For each condition, the diameter of circular polymerised regions was measured, and the results are shown in Fig. **??**, left panel.

The experimental data exhibit a logarithmic relationship between exposure energy and cured diameter. The trend was modelled by the empirical relation:

$$d = m \cdot \ln(I \cdot t) + q$$

where d is the diameter, I is the intensity, t is the time, and m and q are fitting parameters. The fitted equations for each intensity are:

$$\begin{aligned} d_{20} &= 0.8774 \cdot \ln(20 \cdot t) - 4.3641 \\ d_{30} &= 1.0670 \cdot \ln(30 \cdot t) - 6.0205 \\ d_{40} &= 1.2955 \cdot \ln(40 \cdot t) - 7.7595 \end{aligned}$$

These results confirm that increasing light intensity improves lateral resolution by promoting faster crosslinking at the irradiated spot, with minimal diffusion of reactive species beyond the illuminated zone.

In the second set of tests, a formulation containing 0.25% TA was investigated. The hydrogel precursor was exposed to light intensities of 25, 35, and 56 mW/mm^2, and the resulting cured thickness was measured. As shown in Fig. 3.17.B, a similar logarithmic dependence on exposure energy was observed, with the following fitted expressions:

$$\begin{aligned} d_{25} &= 0.8796 \cdot \ln(25 \cdot t) - 5.49882 \\ d_{35} &= 0.91872 \cdot \ln(30 \cdot t) - 6.00105 \\ d_{56} &= 0.40616 \cdot \ln(56 \cdot t) - 2.23892 \end{aligned}$$

Compared to the TA-free samples, the cured layers obtained with 0.25% TA were systematically thinner for equivalent energy inputs. This observation aligns with the role of TA as a UV-absorbing and radical-scavenging additive, which inhibits free radical propagation and slows crosslinking kinetics. Moreover, the material test was instrumental in identifying a suitable range of exposure times and light intensities to be used as a starting point for the subsequent 3D printing trials.

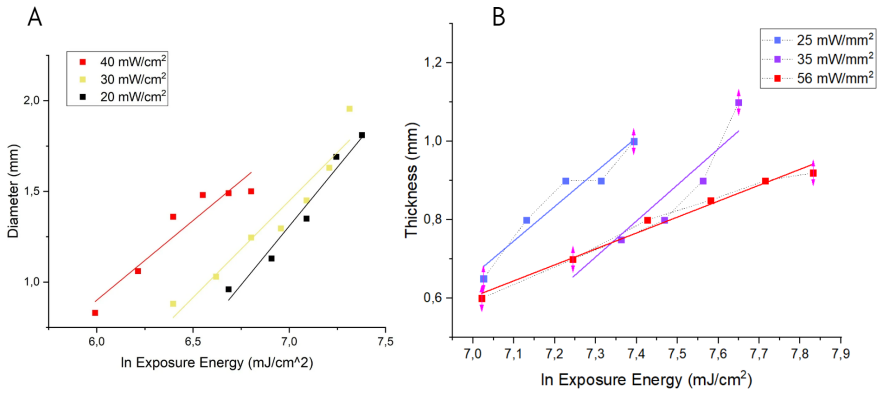

Figure 3.17: (A) Cured diameter of the hydrogel without TA as a function of exposure energy at different light intensities. (B) Cured thickness of the hydrogel containing 0.25% TA. Dotted lines represent logarithmic fits.

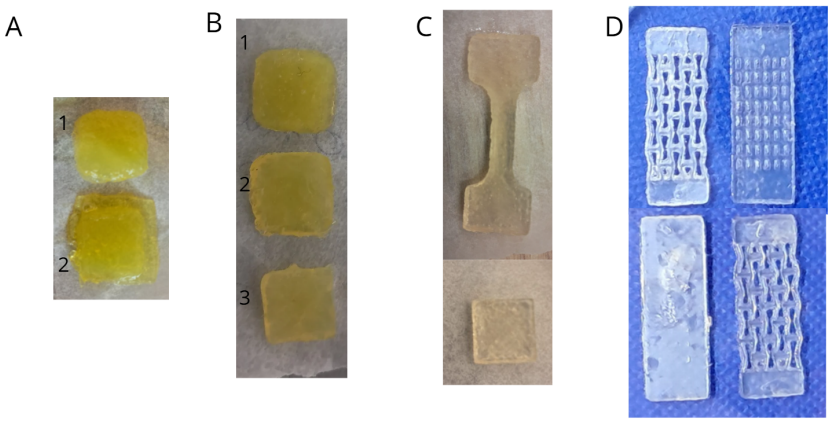

Figure 3.18: Printed samples under different conditions. A) Formulation 1:2 with 20% GelMA and tartrazine, no TA. B) Same formulation as A, with reduced exposure settings. C) Optimised formulation with 0.25% TA. D) Same formulation as C, with fine-tuned parameters for high-resolution printing.

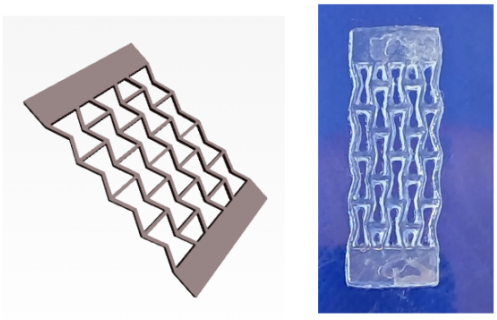

Figure 3.19: Comparison between the designed STL model and the corresponding printed structure obtained with the optimised 0.25% TA formulation (sample D in Fig. 3.18).

3.2 3D printing

To assess the printability of the hydrogel-based formulation, a progressive and iterative experimental approach was adopted. The process began by evaluating the performance of the unmodified hydrogel matrix, and gradually evolved through a series of formulation and parameter refinements that led to a final composition capable of producing high-resolution, structurally robust 3D constructs.

Initially, printing trials were carried out using a GelMA hydrogel at 20% w/v concentration with a 1:4 water/glycerol ratio, incorporating tartrazine as a light-absorbing additive. However, under these conditions, no stable printed structures could be obtained, indicating that the formulation was unsuitable for 3D printing due to inadequate viscosity and mechanical stability.

To overcome this limitation, the formulation was modified by increasing the water/glycerol ratio to 1:2, while keeping the GelMA concentration constant at 20%. This adjustment led to a significant improvement in printability: it was now possible to fabricate structures with defined geometry and layer cohesion. The corresponding results are shown in samples A and B in Fig. 3.18, while the specific printing parameters are summarised in Fig. 3.20. Various combinations of light intensity (from 50 mW/cm^2 to 25 mW/cm^2) and slice thicknesses (from 0.2 mm to 0.02 mm) were tested. Although this revised formulation allowed for basic structure formation, the printed parts still exhibited limited resolution and morphological defects, particularly in the finer geometries. These limitations were likely due to suboptimal mechanical performance and photopolymerisation dynamics under the employed printing conditions.

	Formulation	Light Intensity [mW/cm^2]		Time Exposure [s]	Slice Thickness [mm]
A	0 TA, Tartrazina	1	50	10	0,2
		2	50		0,05
B	0 TA, Tartrazina	1	30	8	0,02
		2	30		0,05
		3	25		0,02
C	0,25 TA	25		20	0,2
D	0,25 TA	5		10	0,02

Figure 3.20: Printing parameters used in the different 3D printing trials.

Subsequently, tannic acid (TA) was incorporated into the system as a multifunctional additive with known capacity to enhance mechanical properties via

non-covalent interactions (e.g., hydrogen bonding and π–π stacking) and to modulate crosslinking density. The inclusion of 0.25% TA (sample C in Fig. 3.18) produced a significant improvement in both printability and mechanical integrity. Even under moderately coarse printing settings (e.g., 25 mW/cm^2, 20 s exposure, 0.2 mm slice height), the resulting structures exhibited greater homogeneity, fewer defects, and improved interlayer bonding. These enhancements were in agreement with the results obtained in rheological characterisation, where TA-containing hydrogels demonstrated increased storage modulus and faster post-exposure gelation kinetics.

The final optimisation phase focused on reducing printing intensity and slice height while preserving fidelity. Using the same 0.25% TA hydrogel formulation but with refined parameters (sample D in Fig. 3.18 and Fig. 3.19 5 mW/cm^2, 10 s exposure, and 0.02 mm slice height), high-resolution structures were successfully fabricated. Notably, the printed constructs included complex lattice geometries, indicating that the system was now capable of supporting the fabrication of intricate patterns with good feature resolution and vertical stacking.

In conclusion, the incorporation of tannic acid not only improved the rheological and mechanical performance of the hydrogel but also expanded the window of printable conditions, enabling reliable 3D printing with low exposure energy and fine slicing—critical features for future biofabrication applications.

3.2.1 Characterisation of printed structures

To evaluate the performance of the printed hydrogel sensors, uniaxial tensile tests were carried out on both standard and structured geometries.

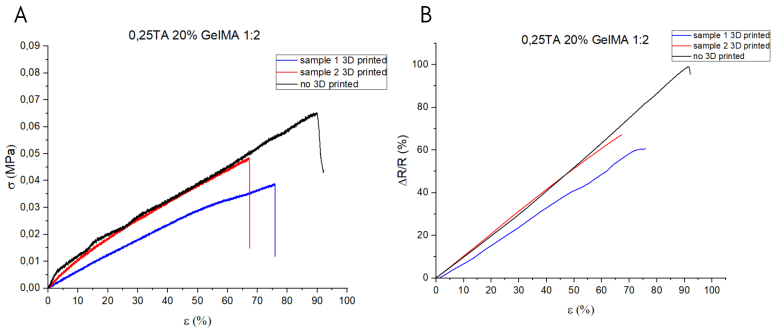

Figure 3.21: Mechanical (A) and electromechanical (B) characterisation of 3D printed and cast-moulded dog-bone samples

As shown in Fig. 3.21, cast-moulded samples (black curves) exhibited the highest mechanical performance, with a linear elastic regime followed by rupture

around 90% strain. In contrast, 3D printed dog-bone samples (red and blue curves) displayed lower failure strains and reduced stiffness, which can be attributed to weak interlayer bonding or incomplete crosslinking between printed layers. This is consistent with the reduction in Young's modulus observed in printed specimens (Fig. 3.23A), where values dropped from approximately 0.16 MPa (moulded) to about 0.14 MPa (3D printed).

Electrically, all samples exhibited a linear $\Delta R/R$ response under strain (Fig. 3.21B). However, the printed samples showed lower maximum $\Delta R/R$ values compared to the moulded ones, likely due to inhomogeneous conductive pathways introduced during printing. Despite this, the printed sensors retained good linearity, validating their functionality for strain-sensing applications.

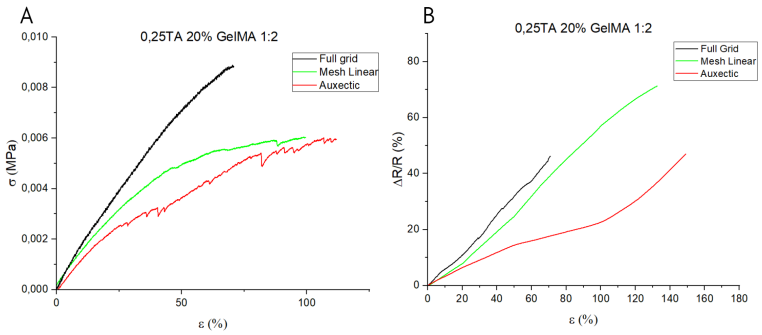

Figure 3.22: Mechanical (A) and electromechanical (B) characterisation of 3D printed sensors with different geometries: full grid (black), mesh linear (green), and auxetic (red).

The influence of printed geometry was further assessed by testing structured samples of equal dimensions (30 mm × 10 mm × 1.5 mm) with three different layouts: full grid (bulk), mesh linear (fine perforations), and auxetic (re-entrant lattice), as shown previously in Fig. 3.18D. The mechanical behaviour (Fig. 3.22A) highlighted that full grid samples exhibited the highest stiffness and stress values. Mesh linear and auxetic samples showed progressively lower mechanical resistance, with the auxetic pattern being the most compliant. This trend was confirmed by the calculated Young's moduli (Fig. 3.23A), with full grid samples reaching approximately 0.03 MPa, and auxetic samples dropping below 0.01 MPa.

From an electromechanical perspective (Fig. 3.22B), the full grid configuration exhibited the highest strain sensitivity among the patterned samples, followed by the mesh linear and auxetic geometries. This behaviour is confirmed by the sensitivity values reported in Fig. 3.23B, where the full grid reached an average sensitivity of approximately 0.9, compared to about 0.75 for mesh linear and 0.55 for auxetic. The lower response of the auxetic structure is attributed to

its increased compliance and distributed deformation, which reduce the effective resistance change. The mesh linear offered a moderate compromise, with improved mechanical flexibility but slightly reduced electrical response compared to the full grid.

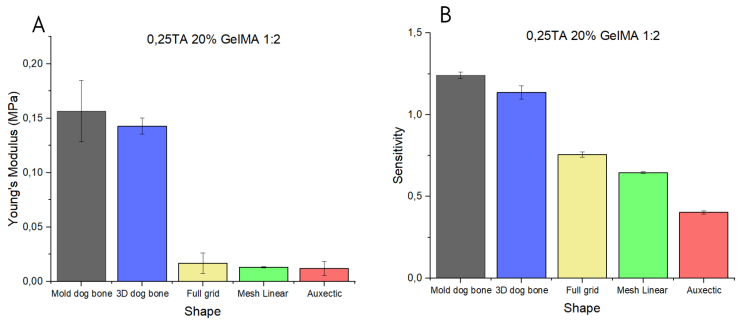

Figure 3.23: Comparison of mechanical (A, Young's modulus) and electrical (B, sensitivity) performance for the different sample types.

The mechanical and electrical performance of the hydrogel-based strain sensors was strongly influenced by both the fabrication method and the structural geometry. Moulded samples showed superior stiffness and sensitivity due to their homogeneous polymer network, but lacked versatility in shape and design.

To further explore the sensing performance under mechanical load, the electromechanical response was plotted as a function of applied stress, as shown in Fig. 3.24. This representation provides a more direct insight into force-sensitive behavior compared to strain-based plots.

The results confirm that all three architectures operate effectively as force sensors, exhibiting progressive resistance increases with applied stress. Among them, the auxetic geometry (red curve) showed the steepest $\Delta R/R$ increase at low stress levels, indicating high responsiveness to minimal forces. However, the signal plateaued rapidly, suggesting early saturation and limited range.

The mesh linear configuration (green curve) displayed a more extended linear regime and moderate sensitivity, offering a balanced performance. The full grid design (black curve) had the lowest sensitivity but the widest linear range, making it more suitable for detecting higher loads without early saturation.

This stress-based analysis reinforces the prior strain-based findings (Fig. 3.22B), highlighting how the auxetic design excels in detecting low forces, while the full grid structure maintains robustness under larger loads. The mesh linear once again emerges as a geometrically favorable compromise, balancing deformation capacity and electrical signal stability across a broad range of mechanical stimuli.

These observations confirm that not only the material formulation but also the printed geometry plays a critical role in tuning the mechanical–electrical coupling

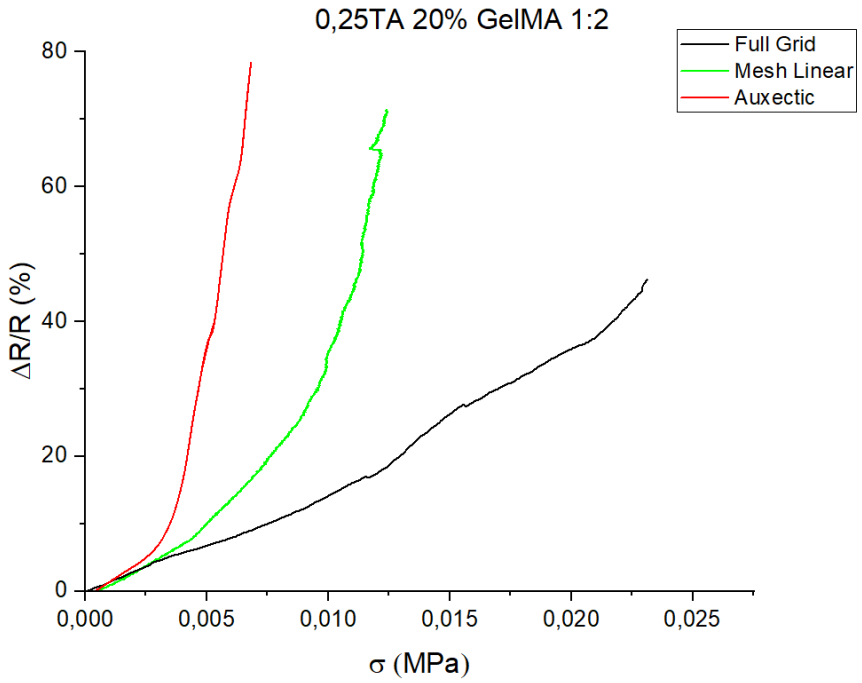

Figure 3.24: Electromechanical response ($\Delta R/R$ vs applied stress) of 3D printed sensors with different geometries: full grid (black), mesh linear (green), and auxetic (red).

of hydrogel-based sensors. The ability to modulate sensitivity and working range through design strategies underscores the versatility of 3D printing for customising sensor behaviour in wearable and soft electronics applications.

3.3 Functional testing for wearable sensing

To validate the applicability of the developed hydrogel-based strain sensors in real-world scenarios, a set of functional tests was performed by directly attaching the devices to human skin. These tests involved dynamic and static mechanical deformations of various body parts and were designed to evaluate signal fidelity, response linearity, and detection sensitivity under physiological conditions.

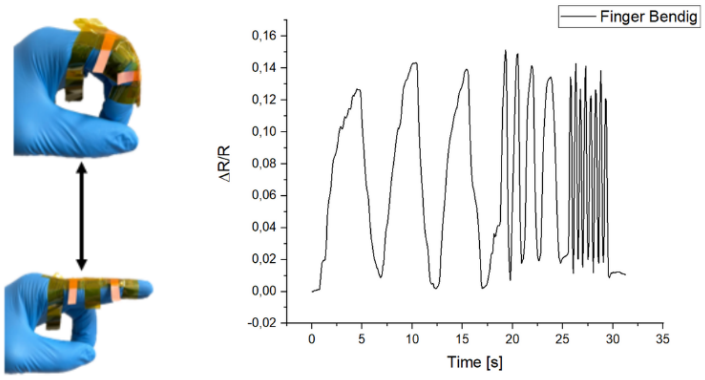

Figure 3.25: Real-time monitoring of repetitive finger bending at different frequencies using a printed hydrogel strain sensor.

Fig. 3.25 shows the electromechanical response of the sensor placed over a finger joint subjected to repeated bending and extension. The $\Delta R/R$ signal follows the cyclic motion with high reproducibility, maintaining a clear and well-defined peak for each bending cycle. Notably, the increase in frequency after 20 s leads to a higher oscillation rate without loss of signal quality, confirming the sensor's responsiveness and ability to track dynamic deformation in real time.

In Fig. 3.26, the sensor was subjected to incremental angular deformation by bending the finger to distinct positions. Each step in the plot corresponds to a new fixed angle, and the $\Delta R/R$ signal displays a proportional increase with each bending level. The plateau-like behaviour observed at each stage demonstrates the sensor's stability in static conditions and its potential for postural monitoring.

Fig. 3.27 presents the response obtained from placing the sensor on the forearm, over the muscle groups responsible for finger actuation. Periodic muscle contractions induced by finger movement generate distinct peaks in the $\Delta R/R$ signal. The

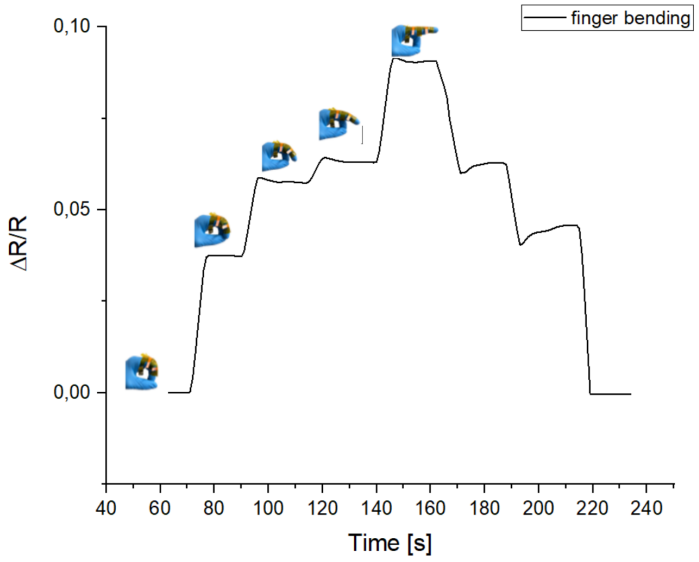

Figure 3.26: Stepwise resistance change as the finger is held at different angular positions.

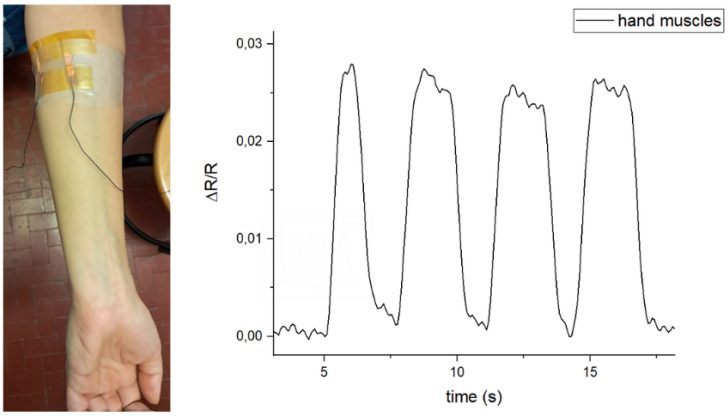

Figure 3.27: Electromechanical response of the sensor attached to the forearm during hand muscle actuation (finger movement).

sensor was able to detect subtle deformations associated with muscular activity, confirming its effectiveness in remote strain detection beyond direct joint movement.

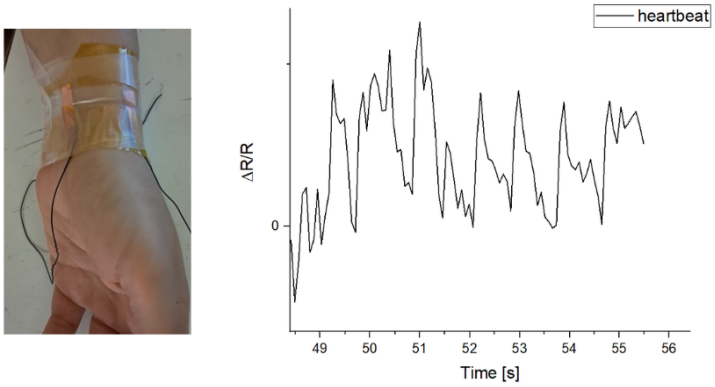

Figure 3.28: Detection of wrist pulse via resistance variation.

Pulse monitoring capability was evaluated by placing the sensor over the radial artery at the wrist (Fig. 3.28). The sensor successfully captured small periodic resistance changes corresponding to heartbeat-induced pressure waves. The signal exhibits a frequency of approximately 1.1 Hz, equivalent to a heart rate of about 66 beats per minute (bpm), which falls within the physiological resting range for adults. The waveform exhibits consistent periodicity, demonstrating the device's capability to monitor subtle physiological signals.

Overall, these results demonstrate the versatility of the 3D printed hydrogel strain sensors in detecting a broad range of human motions—from large-scale joint bending to fine physiological signals such as muscle activation and arterial pulse. The sensors showed consistent response, good signal-to-noise ratio, and robustness under both dynamic and static conditions, highlighting their potential for wearable applications in motion tracking, rehabilitation monitoring, and personalised healthcare.

Overall, these results demonstrate the versatility of the studied sensor in detecting a wide range of human motion, from large-scale joint flexion to precise physiological signals such as muscle activation and arterial pulsation. The sensors demonstrated consistent response, good signal-to-noise ratio, and robustness in both dynamic and static conditions, highlighting their potential for wearable applications in motion monitoring, rehabilitation monitoring, and personalized healthcare.

Chapter 4

Conclusion

This work presented the formulation, fabrication, and characterisation of GelMA-based hydrogel strain sensors enhanced by tannic acid (TA) and manufactured via digital light processing (DLP) 3D printing. The goal was to create a soft, biocompatible, and conductive material platform capable of high-resolution fabrication and reliable strain sensing for wearable applications.

The hydrogel matrix was formulated using GelMA as the structural polymer, glycerol as a biocompatible, non-volatile solvent, and NaCl as the ionic conductor. In particular, the use of glycerol was key to overcoming the typical drawback of hydrogel-based sensors: water evaporation. By replacing part of the water phase with glycerol, the formulation exhibited enhanced long-term stability, maintaining its mechanical and electrical properties even after prolonged storage under ambient conditions. This characteristic is especially important for wearable applications, where the sensor may be subjected to variable environmental conditions without protection.

The addition of tannic acid further improved the system, acting as a multifunctional additive that contributed to network reinforcement, crosslinking efficiency, and surface adhesion.

The experimental results confirmed the validity of the proposed strategy across several key aspects:

- **Role of tannic acid:** The introduction of tannic acid at an optimised concentration of 0.25% w/w (with respect to the total formulation) proved crucial in improving both the mechanical robustness and the environmental stability of the hydrogel network. Rheological characterisation revealed a marked increase in the storage modulus (G'), indicating a more elastic and stable structure. Photorheological studies demonstrated that TA slightly delayed the onset of gelation, but led to more efficient crosslinking, compatible

with the requirements of DLP-based 3D printing. In addition, adhesion tests showed that TA enhanced bonding to various substrates such as glass, metal, and wood—an important property for real-world integration.

- **Printability and structural resolution:** TA-containing formulations enabled the successful printing of structures that were otherwise unprintable using unmodified GelMA. Initial trials with 1:4 water/glycerol formulations proved inadequate due to poor mechanical integrity and low viscosity. The transition to a 1:2 water/glycerol formulation, combined with 0.25% TA, provided the rheological properties needed to support high-resolution printing. Notably, it was possible to produce complex lattice structures such as auxetic and mesh geometries with fine layer thickness (0.02 mm) and low light intensity (5 mW/cm^2), achieving well-defined features and high printing fidelity.

- **Mechanical and electrical performance:** Tensile tests revealed that the printed samples—while slightly less stiff than their cast-moulded counterparts—retained sufficient mechanical strength for practical use. The best-performing printed structures exhibited Young's moduli in the range of 0.12–0.14 MPa and failure strains exceeding 50%, depending on geometry. Electromechanical characterisation confirmed a linear $\Delta R/R$ response to strain, with sensitivities up to 0.9 for the mesh linear configuration. The auxetic design, while more deformable, showed lower electrical sensitivity, and the full grid structure provided higher mechanical stiffness but lower relative variation in resistance. These results highlight the importance of optimising both material composition and geometry to balance stretchability and signal output.

- **Application potential:** Functional validation confirmed the sensor's applicability to real-world deformation detection. When applied to the skin, the device reliably detected finger motion at different frequencies and angles, as well as muscle contractions in the forearm. Notably, the sensor was also able to detect wrist pulse signals, with consistent and periodic $\Delta R/R$ traces that reflected the cardiac rhythm (around 66 bpm). These demonstrations illustrate the sensor's capability to capture both macroscopic body movements and subtle physiological activity with a good signal-to-noise ratio.

In conclusion, this thesis demonstrated that a tailored combination of glycerol-based ionic GelMA hydrogel, reinforced with tannic acid and structured via high-resolution 3D printing, can yield a soft, conductive, and functionally robust platform

suitable for wearable strain sensing. The proposed approach enables the realisation of fully customisable, biocompatible sensors that offer mechanical flexibility, printability, and long-term stability—key features for the next generation of soft bioelectronic systems.

Future Developments

Building upon the findings of this work, several future directions may be pursued to further enhance the functionality, versatility, and application scope of GelMA-based hydrogel sensors:

- **Multimaterial and multimodal integration:** Future studies could explore the incorporation of multiple functional materials within the same hydrogel matrix or in layered configurations, enabling simultaneous detection of different stimuli (e.g., strain, pressure, temperature). Such multimodal sensing platforms could leverage localised differences in composition to create spatially programmable responses.
- **Expansion to other sensing modalities:** Beyond strain sensing, the platform could be adapted for additional signal transduction mechanisms. For instance, ionic thermoresponsive elements or conductive nanocomposites could be introduced to enable temperature or pressure sensing. This would broaden the range of biomedical or environmental parameters that can be monitored with a single device.
- **Triboelectric enhancement:** The design could be extended to incorporate triboelectric elements, allowing energy harvesting from mechanical motion. Combining triboelectric nanogenerators (TENGs) with soft conductive hydrogels may yield self-powered sensing systems suitable for remote or implantable use.
- **Integration and miniaturisation for biomedical applications:** Future developments should focus on device miniaturisation and integration with soft electronics or wireless modules. This would enable real-time monitoring in applications such as wearable rehabilitation systems, joint tracking, or smart orthopaedic devices. The inherent softness and biocompatibility of the developed hydrogels make them suitable for minimally invasive, skin-conformal, or even implantable implementations.

Bibliography

[1] Ali Raza, Hasan Zulfiqar, Zheng Gong, Yanzheng Chen, and Yifan Chen. «A Comprehensive Review on Biomedical Sensors: Technological Advancements, Applications in Molecular Informatics, and Future Trends». In: *Preprints* 202410.1645 (2024). This version is not peer-reviewed (cit. on p. 2).

[2] Ayan Kumar Panja, Amartya Mukherjee, and Nilanjan Dey. «Chapter 1 - Introduction». In: *Biomedical Sensors and Smart Sensing*. Ed. by Ayan Kumar Panja, Amartya Mukherjee, and Nilanjan Dey. Primers in Biomedical Imaging Devices and Systems. Academic Press, 2022, pp. 1–14. ISBN: 978-0-12-822856-2 (cit. on p. 2).

[3] «Recent developments in biosensors for healthcare and biomedical applications: A review». In: *Measurement* 167 (2021), p. 108293. ISSN: 0263-2241 (cit. on p. 2).

[4] Yu-Hsin Chang, Ching-Cheng Chang, Ling-Yu Chang, Pang-Chen Wang, Pawisa Kanokpaka, and Min Yen Yeh. «Self-powered triboelectric sensor with N-doped graphene quantum dots decorated polyaniline layer for non-invasive glucose monitoring in human sweat». In: *Nano Energy* 112 (2023), p. 108505 (cit. on p. 3).

[5] Bouchaib Zazoum, Khalid Mujasam Batoo, and Muhammad Azhar Ali Khan. «Recent Advances in Flexible Sensors and Their Applications». In: *Sensors* 22.12 (2022) (cit. on p. 3).

[6] Pan Jiang, Zhongying Ji, Xiaoqin Zhang, Zhilu Liu, and Xiaolong Wang. «Recent advances in direct ink writing of electronic components and functional devices». In: *Progress in Additive Manufacturing* 3.1 (2018), pp. 65–86 (cit. on p. 3).

[7] Xuchu Dong, Yong Wei, Song Chen, Yong Lin, Lan Liu, and Jing Li. «A linear and large-range pressure sensor based on a graphene/silver nanowires nanobiocomposites network and a hierarchical structural sponge». In: *Composites Science and Technology* 155 (2018), pp. 108–116 (cit. on p. 3).

[8] Sam Ali, Dinesh Maddipatla, Binu Baby Narakathu, Amer A Chlaihawi, Sepehr Emamian, Farah Janabi, Bradley J Bazuin, and Massood Z Atashbar. «Flexible capacitive pressure sensor based on PDMS substrate and Ga–In liquid metal». In: *IEEE Sensors Journal* 19.1 (2018), pp. 97–104 (cit. on p. 3).

[9] Taemin Lee, Wonoh Lee, Sung-Woo Kim, Jae Joon Kim, and Byeong-Su Kim. «Flexible textile strain wireless sensor functionalized with hybrid carbon nanomaterials supported ZnO nanowires with controlled aspect ratio». In: *Advanced Functional Materials* 26.34 (2016), pp. 6206–6214 (cit. on p. 3).

[10] Patrik Sobolčiak, Aisha Tanvir, Kishor Kumar Sadasivuni, and Igor Krupa. «Piezoresistive sensors based on electrospun mats modified by 2D Ti3C2Tx MXene». In: *Sensors* 19.20 (2019), p. 4589 (cit. on p. 4).

[11] Ziya Wang, Xiao Guan, Huayi Huang, Haifei Wang, Waner Lin, and Zhengchun Peng. «Full 3D printing of stretchable piezoresistive sensor with hierarchical porosity and multimodulus architecture». In: *Advanced Functional Materials* 29.11 (2019), p. 1807569 (cit. on p. 4).

[12] Jun Shintake, Yegor Piskarev, Seung Hee Jeong, and Dario Floreano. «Ultrastretchable strain sensors using carbon black-filled elastomer composites and comparison of capacitive versus resistive sensors». In: *Advanced Materials Technologies* 3.3 (2018), p. 1700284 (cit. on p. 4).

[13] Evgenia P Gilshteyn, Stepan A Romanov, Daria S Kopylova, Georgy V Savostyanov, Anton S Anisimov, Olga E Glukhova, and Albert G Nasibulin. «Mechanically tunable single-walled carbon nanotube films as a universal material for transparent and stretchable electronics». In: *ACS applied materials interfaces* 11.30 (2019), pp. 27327–27334 (cit. on p. 4).

[14] Yalong Wang, Ji Hao, Zhenqi Huang, Guoqiang Zheng, Kun Dai, Chuntai Liu, and Changyu Shen. «Flexible electrically resistive-type strain sensors based on reduced graphene oxide-decorated electrospun polymer fibrous mats for human motion monitoring». In: *Carbon* 126 (2018), pp. 360–371 (cit. on p. 4).

[15] Michał Rycewicz, Mateusz Ficek, Krzysztof Gajewski, Srinivasu Kunuku, Jakub Karczewski, Teodor Gotszalk, I Wlasny, Andrzej Wysmołek, and Robert Bogdanowicz. «Low-strain sensor based on the flexible boron-doped diamond-polymer structures». In: *Carbon* 173 (2021), pp. 832–841 (cit. on p. 4).

[16] Li Tang, Shaoji Wu, Jie Qu, Liang Gong, and Jianxin Tang. «A Review of Conductive Hydrogel Used in Flexible Strain Sensor». In: *Materials* 13.18 (2020) (cit. on pp. 4, 5).

[17] Chunqing Yang, Weiwei Wang, Dongzhi Zhang, Chen Du, Hao Zhang, and Hui Xia. «High-Sensitivity Wearable Flexible Pressure Sensor Based on MXene and Polyaniline for Human Motion Detection». In: *ACS Applied Polymer Materials* 5.12 (2023), pp. 10386–10394 (cit. on p. 6).

[18] David Seliktar. «Designing cell-compatible hydrogels for biomedical applications». In: *Science* 336.6085 (2012), pp. 1124–1128 (cit. on p. 6).

[19] Sakshi B. Bhalerao, Vijay R. Mahajan, and Rahul R. Maske. «Hydrogel based drug delivery system: A review». In: *World Journal of Biology Pharmacy and Health Sciences* 12.03 (2022), pp. 039–053 (cit. on p. 6).

[20] Nicholas A. Peppas, Y. Huang, M. Torres-Lugo, J. H. Ward, and J. Zhang. «Physicochemical foundations and structural design of hydrogels in medicine and biology». In: *Annual Review of Biomedical Engineering* 2 (2000), pp. 9–29 (cit. on p. 6).

[21] A. Onaciu, R. A. Munteanu, A. I. Moldovan, C. S. Moldovan, and I. Berindan-Neagoe. «Hydrogels Based Drug Delivery: Synthesis, Characterization and Administration». In: *Pharmaceutics* 11 (2019), p. 432 (cit. on p. 6).

[22] Enas M. Ahmed. «Hydrogel: Preparation, characterization, and applications: A review». In: *Journal of Advanced Research* 6.2 (2015), pp. 105–121. ISSN: 2090-1232 (cit. on p. 6).

[23] J.Y. Sun, X. Zhao, W. Illeperuma, and et al. «Highly stretchable and tough hydrogels». In: *Nature* 489 (2012), pp. 133–136 (cit. on p. 7).

[24] Wei Seong Toh and Xian Jun Loh. «Advances in hydrogel delivery systems for tissue regeneration». In: *Materials Science and Engineering: C* 45 (2014), pp. 690–697. ISSN: 0928-4931 (cit. on p. 7).

[25] Yulia Berkovitch and Dror Seliktar. «Semi-synthetic hydrogel composition and stiffness regulate neuronal morphogenesis». In: *International Journal of Pharmaceutics* 523.2 (2017), pp. 545–555 (cit. on p. 7).

[26] Xiaoxu Liang, Minghui Zhang, Cheong-Meng Chong, Danlei Lin, Shiji Chen, Yumiao Zhen, Hongyao Ding, and Hai-Jing Zhong. «Recent Advances in the 3D Printing of Conductive Hydrogels for Sensor Applications: A Review». In: *Polymers* 16.15 (2024) (cit. on pp. 7, 12, 18–20).

[27] Brian W Walker, Roberto Portillo Lara, Emad Mogadam, Chu Hsiang Yu, William Kimball, and Nasim Annabi. «Rational design of microfabricated electroconductive hydrogels for biomedical applications». In: *Progress in polymer science* 92 (2019), pp. 135–157 (cit. on p. 7).

[28] Hyunwoo Yuk, Baoyang Lu, and Xuanhe Zhao. «Hydrogel bioelectronics». In: *Chemical Society Reviews* 48.6 (2019), pp. 1642–1667 (cit. on pp. 7, 10).

[29] Yuxi Xu, Kaixuan Sheng, Chun Li, and Gaoquan Shi. «Self-assembled graphene hydrogel via a one-step hydrothermal process». In: *ACS nano* 4.7 (2010), pp. 4324–4330 (cit. on p. 8).

[30] BY Lu, H Yuk, ST Lin, NN Jian, K Qu, JK Xu, and XH Zhao. *Pure PEDOT: PSS hydrogels. Nat Commun 10 (1): 1043.* 2019 (cit. on p. 8).

[31] Dong Liu et al. «A Strand Entangled Supramolecular PANI/PAA Hydrogel Enabled Ultra-Stretchable Strain Sensor». In: *Small* 18.47 (), p. 2203258 (cit. on pp. 8, 9).

[32] Dong Liu et al. «A strand entangled supramolecular PANI/PAA hydrogel enabled ultra-stretchable strain sensor». In: *Small* 18.47 (2022), p. 2203258 (cit. on p. 8).

[33] Yinjie Peng, Menghan Pi, Xiaoling Zhang, Bin Yan, Yueshan Li, Lingying Shi, and Rong Ran. «High strength, antifreeze, and moisturizing conductive hydrogel for human-motion detection». In: *Polymer* 196 (2020), p. 122469 (cit. on p. 8).

[34] Yang Zhou et al. «Highly stretchable, elastic, and ionic conductive hydrogel for artificial soft electronics». In: *Advanced Functional Materials* 29.1 (2019), p. 1806220 (cit. on p. 8).

[35] Siheng Wang, Le Yu, Shanshan Wang, Lei Zhang, Lu Chen, Xu Xu, Zhanqian Song, He Liu, and Chaoji Chen. «Strong, tough, ionic conductive, and freezing-tolerant all-natural hydrogel enabled by cellulose-bentonite coordination interactions». In: *Nature Communications* 13.1 (2022), p. 3408 (cit. on pp. 9, 10).

[36] «A semi-interpenetrating network ionic composite hydrogel with low modulus, fast self-recoverability and high conductivity as flexible sensor». In: *Carbohydrate Polymers* 248 (2020), p. 116797 (cit. on p. 10).

[37] «High-strength and highly electrically conductive hydrogels for wearable strain sensor». In: *Chemical Physics Letters* 769 (2021), p. 138437. ISSN: 0009-2614 (cit. on p. 11).

[38] Yan-Jun Liu, Wen-Tao Cao, Ming-Guo Ma, and Pengbo Wan. «Ultrasensitive wearable soft strain sensors of conductive, self-healing, and elastic hydrogels with synergistic "soft and hard" hybrid networks». In: *ACS Applied Materials & Interfaces* 9.29 (2017), pp. 25559–25570 (cit. on p. 12).

[39] R. Xing, Y. Liu, Q. Zhang, J. Li, Y. Zhang, and P. Li. «An All-in-One Tannic Acid-Containing Hydrogel Adhesive with High Toughness, Notch Insensitivity, Self-Healability, Tailorable Topography, and Strong, Instant, and On-Demand Underwater Adhesion». In: *ACS Applied Materials & Interfaces* 13.8 (2021), pp. 9748–9761 (cit. on p. 13).

[40] Sondos Dbira, Nasr Bensalah, Moustafa Zagho, Massouda Ennahaoui, and Ahmed Bedoui. «Oxidative Degradation of Tannic Acid in Aqueous Solution by UV/S2O8 and UV/H2O2/Fe Processes: A Comparative Study». In: *Applied Sciences* 9 (Jan. 2019), p. 156 (cit. on p. 13).

[41] K. Kim, M. Shin, M. Y. Koh, J. H. Ryu, M. S. Lee, S. Hong, and H. Lee. «TAPE: A Medical Adhesive Inspired by a Ubiquitous Compound in Plants». In: *Advanced Functional Materials* 25.16 (2015), pp. 2402–2410 (cit. on p. 13).

[42] «A tough shape memory hydrogel strain sensor based on gelatin grafted polypyrrole». In: *Polymer* 263 (2022), p. 125524. ISSN: 0032-3861 (cit. on pp. 13, 14).

[43] Chunxia Zhao, Yunxin Chen, Min Guo, Yuanpeng Wu, Yuntao Li, Dong Xiang, Hui Li, Li Wang, and Zhe Sun. «Flexible, adhesive, strain-sensitive, and skin-matchable hydrogel strain sensors for human motion and handwritten signal monitoring». In: *Polymers for Advanced Technologies* 34.1 (2022), pp. 430–440 (cit. on p. 15).

[44] Zhen Li, Shanshan Zhang, Yujie Chen, Haotian Ling, Xuan Wang, Michael C. Hartel, and Ali Khademhosseini. «Gelatin Methacryloyl-Based Tactile Sensors for Medical Wearables». In: *Advanced Functional Materials* 30.49 (2020), p. 2003601 (cit. on p. 15).

[45] Kai Yue, Guillermo Trujillo-de Santiago, María M. Alvarez, Ali Tamayol, Nasim Annabi, and Ali Khademhosseini. «Synthesis, Properties, and Biomedical Applications of Gelatin Methacryloyl (GelMA) Hydrogels». In: *Biomaterials* 73 (2015), pp. 254–271 (cit. on pp. 15, 23).

[46] Sasinan Bupphathong, Carlos Quiroz, Wei Huang, Pei-Feng Chung, Hsuan-Ya Tao, and Chih-Hsin Lin. «Gelatin Methacrylate Hydrogel for Tissue Engineering Applications—A Review on Material Modifications». In: *Pharmaceuticals* 15.2 (2022) (cit. on p. 16).

[47] Franziska B. Albrecht, Freia F. Schmidt, Ann-Cathrin Volz, and Petra J. Kluger. «Bioprinting of 3D Adipose Tissue Models Using a GelMA-Bioink with Human Mature Adipocytes or Human Adipose-Derived Stem Cells». In: *Gels* 8.10 (2022) (cit. on p. 16).

[48] Jingyi Liu, Bin Zhang, Liang Li, Jun Yin, and Fu Jianzhong. «Additive-lathe 3D bioprinting of bilayered nerve conduits incorporated with supportive cells». In: *Bioactive Materials* 6 (Jan. 2021), pp. 219–229 (cit. on p. 16).

[49] Qi Zhang et al. «Ultrasoft and Biocompatible Magnetic-Hydrogel-Based Strain Sensors for Wireless Passive Biomechanical Monitoring». In: *ACS Nano* 16.12 (2022), pp. 21555–21564 (cit. on p. 17).

[50] «Hydrogen bonds autonomously powered gelatin methacrylate hydrogels with super-elasticity, self-heal and underwater self-adhesion for sutureless skin and stomach surgery and E-skin». In: *Biomaterials* 171 (2018), pp. 83–96 (cit. on pp. 17, 18, 44).

[51] «3D printing of electrically conductive and degradable hydrogel for epidermal strain sensor». In: *Composites Communications* 37 (2023), p. 101454. ISSN: 2452-2139 (cit. on pp. 18, 21).

[52] Zhe Chen, Donghao Zhao, Binhong Liu, Guodong Nian, Xiaokeng Li, Jun Yin, Shaoxing Qu, and Wei Yang. «3D Printing of Multifunctional Hydrogels». In: *Advanced Functional Materials* 29.20 (2019), p. 1900971 (cit. on pp. 18, 21, 23).

[53] «3D printed electronics: Processes, materials and future trends». In: *Progress in Materials Science* 127 (2022), p. 100945 (cit. on p. 18).

[54] CW Hull. *Apparatus for production of three-dimensional objects by stereolithography. US 4575330 A, Google Patents*. 1986 (cit. on p. 18).

[55] «3D printing of polymer composites: Materials, processes, and applications». In: *Matter* 5.1 (2022), pp. 43–76. ISSN: 2590-2385 (cit. on p. 18).

[56] Naroa Lopez-Larrea, Antonela Gallastegui, Luis Lezama, Miryam Criado-Gonzalez, Nerea Casado, and David Mecerreyes. «Fast Visible-Light 3D Printing of Conductive PEDOT:PSS Hydrogels». In: *Macromolecular Rapid Communications* 45.1 (), p. 2300229 (cit. on p. 18).

[57] E Taneva, B Kusnoto, and CA Evans. *3D Scanning, Imaging, and Printing in Orthodontics: Issues in Contemporary Orthodontics. Prof. Farid Bourzgui (ed.), London, UK*. 2015 (cit. on p. 19).

[58] Ethan Berger et al. «Recent developments in perovskite-based precursor inks for scalable architectures of perovskite solar cell technology». In: *Sustainable Energy and Fuels* 6 (May 2022) (cit. on p. 19).

[59] «Three-dimensional printing of multilayered tissue engineering scaffolds». In: *Materials Today* 21.8 (2018), pp. 861–874 (cit. on p. 19).

[60] Xiangren Kong, Min Dong, Miao Du, Jin Qian, Jun Yin, Qiang Zheng, and Zi Liang Wu. «Recent Progress in 3D Printing of Polymer Materials as Soft Actuators and Robots». In: *Chem & Bio Engineering* 1.4 (2024), pp. 312–329 (cit. on pp. 19, 20).

[61] M. N. M. Azlin, R. A. Ilyas, M. Y. M. Zuhri, S. M. Sapuan, M. M. Harussani, Shubham Sharma, A. H. Nordin, N. M. Nurazzi, and A. N. Afiqah. «3D Printing and Shaping Polymers, Composites, and Nanocomposites: A Review». In: *Polymers* 14.1 (2022) (cit. on p. 20).

[62] Matteo Caprioli, Ignazio Roppolo, Annalisa Chiappone, Liraz Larush, Candido Fabrizio Pirri, and Shlomo Magdassi. «3D-printed self-healing hydrogels via Digital Light Processing». In: *Nature Communications* 12.1 (2021), p. 2462 (cit. on p. 22).

[63] Rudra Nath Ghosh, Joseph Thomas, Vaidehi B. R., Devi N. G., Akshitha Janardanan, Pramod K. Namboothiri, and Mathew Peter. «An insight into synthesis, properties and applications of gelatin methacryloyl hydrogel for 3D bioprinting». In: *Mater. Adv.* 4 (22 2023), pp. 5496–5529 (cit. on pp. 22, 23).

[64] Tanmay Jain, Hannah B. Baker, Anna Gipsov, John P. Fisher, Abraham Joy, David S. Kaplan, and Irada Isayeva. «Impact of cell density on the bioprinting of gelatin methacrylate (GelMA) bioinks». In: *Bioprinting* 22 (Feb. 2021), e00131 (cit. on p. 23).

[65] Sina Sharifi, Hannah Sharifi, Ali Akbari, and James Chodosh. «Systematic optimization of visible light-induced crosslinking conditions of gelatin methacryloyl (GelMA)». In: *Scientific Reports* 11.1 (2021), p. 23276 (cit. on pp. 23, 24).

[66] Ping Song et al. «DLP fabricating of precision GelMA/HAp porous composite scaffold for bone tissue engineering application». In: *Composites Part B Engineering* 244 (Aug. 2022), p. 110163 (cit. on p. 24).

[67] Khoon S. Lim, Barbara J. Klotz, Gabriella C. J. Lindberg, Ferry P. W. Melchels, Gary J. Hooper, Jos Malda, Debby Gawlitta, and Tim B. F. Woodfield. «Visible Light Cross-Linking of Gelatin Hydrogels Offers an Enhanced Cell Microenvironment with Improved Light Penetration Depth». In: *Macromolecular Bioscience* 19.6 (Apr. 2019) (cit. on p. 24).

[68] Gozde Basara, Xiaoshan Yue, and Pinar Zorlutuna. «Dual Crosslinked Gelatin Methacryloyl Hydrogels for Photolithography and 3D Printing». In: *Gels* 5.3 (2019) (cit. on p. 25).

[69] Huimin Shi, Yang Li, Kailei Xu, and Jun Yin. «Advantages of photo-curable collagen-based cell-laden bioinks compared to methacrylated gelatin (GelMA) in digital light processing (DLP) and extrusion bioprinting». In: *Materials Today Bio* 23 (2023), p. 100799 (cit. on pp. 25–27).

[70] Wendan Jia, Zixian Liu, Lei Sun, Yanyan Cao, Zhizhong Shen, Meng Li, Yang An, Hulin Zhang, and Shengbo Sang. «A multicrosslinked network composite hydrogel scaffold based on DLP photocuring printing for nasal cartilage repair». In: *Biotechnology and Bioengineering* 121.9 (2024), pp. 2752–2766 (cit. on p. 27).

[71] Yang Li, Qijiang Mao, Xiaokeng Li, Jun Yin, Yifang Wang, Jianzhong Fu, and Yong Huang. «High-fidelity and high-efficiency additive manufacturing using tunable pre-curing digital light processing». In: *Additive Manufacturing* 30 (2019), p. 100889 (cit. on p. 28).

[72] Margaux Vigata, Christoph Meinert, Stephen Pahoff, Nathalie Bock, and Dietmar W. Hutmacher. «Gelatin Methacryloyl Hydrogels Control the Localized Delivery of Albumin-Bound Paclitaxel». In: *Polymers* 12.2 (2020) (cit. on p. 29).